



UNIVERSITAT POLITÈCNICA
DE CATALUNYA
BARCELONATECH

UWB for medical applications

A Degree Thesis

**Submitted to the Faculty of the
Escola Tècnica d'Enginyeria de Telecomunicació de
Barcelona**

Universitat Politècnica de Catalunya

by

Guillermo Rodríguez Serra

**In partial fulfilment
of the requirements for the degree in
SCINCE AND TELECOMUNICATION
TECHNOLOGIES ENGINEERING**

Advisor: Montse Nájara and Mònica Navarro

Barcelona, October 2015

Abstract

The respiratory frequency monitoring is an important indicator to the medical field. Also, the need of sensor system solutions for home monitoring is growing as the life expectancy of the world population is increasing. For those reasons, this thesis considers the use of an impulse-radio (IR) UWB radar system to track respiratory frequency and respiratory patterns, as apnoea episodes, in a non-invasive and real-time way. We start our analysis with well-known spectral estimators, like the Periodogram or Bartlett estimator to obtain the first results and insights over the estimation of steady frequencies in an offline regime. Later, we consider the use of adaptive algorithms like the LMS together with AR modelling to monitor the breathing rate transitions and variations. Simulations have been performed to validate and adjust the parameters of the algorithms, balancing between its trade-offs to suit our solution to the problem. Finally, the results of the experiments in different environments are presented meeting the expected requirements and performance of the system.

Resum

La monitorització de la freqüència respiratòria es un important indicador en el camp de la medicina. De la mateixa manera, la necessitat de solucions basades en sistemes de sensors per a monitoritzar pacients no hospitalitzats a les seves llars creix a mesura que la esperança de vida de la població mundial creix. Per aquestes raons, aquesta tesi considera l'ús d'un sistema de radar basat en impulse-radio (IR) UWB per a controlar la freqüència respiratòria, i al mateix temps, patrons de respiració, com episodis d'apnea, d'una manera no invasiva i a temps real. Comencem el nostre anàlisi amb estimadors espectrals com el Periodograma o l'Estimador Bartlett per a obtenir els primers resultats en l'estimació de freqüències estables en una configuració no en temps real, per continuar amb, l'ús d'algoritmes adaptatius com LMS junt a modelat AR per a monitoritzar les transicions y variacions en la freqüència respiratòria. Hem dut a terme simulacions per a validar i ajustar els paràmetres dels algoritmes, intentant compensar les seves diferents característiques per a ajustar-los a la nostra problemàtica. Finalment, els resultats de experiments en diferent escenaris son presentats acomplint amb els requisits i rendiments esperats del sistema.

Resumen

La monitorización de la frecuencia respiratoria es un importante indicador en el campo de la medicina. De la misma manera, la necesidad de soluciones basadas en sistemas de sensores para monitorizar pacientes no hospitalizados en sus hogares crece al mismo ritmo que la esperanza de vida de la población mundial crece. Por esas razones, esta tesis considera el uso de un sistema de radar basado en impulse-radio (IR) UWB para controlar la frecuencia respiratoria, y a la vez, patrones respiratorios, como episodios de apnea, de una manera no invasiva y a tiempo real. Empezamos nuestro análisis con estimadores espectrales como el Periodograma o Estimador Bartlett para obtener los primeros resultados en la estimación de frecuencias estables en una configuración no en tiempo real. Más tarde, consideramos el uso de algoritmos adaptativos como LMS junto a modelado AR para monitorizar las transiciones y variaciones en la frecuencia respiratoria. Se han llevado a cabo simulaciones para validar y ajustar los parámetros de los algoritmos, intentando compensar sus diferentes características para ajustarlos a nuestra problemática. Finalmente, los resultados de experimentos en diferentes escenarios son presentados cumpliendo con los requerimientos y rendimientos esperados del sistema.

Acknowledgements

I want to acknowledge the collaboration and hospitality of the staff at the Centre Tecnològic Telecomunicacions Catalunya (CTTC), in special to Mònica Navarro, Pau Closas and Ana Moragrega. Also the opportunity to work in a research centre and been allowed to use the needed hardware tools to develop my thesis has been a great experience.

And finally many thanks to Montse Nájjar and Mònica Navarro for her help and guidance throughout all this thesis.

Revision history and approval record

Revision	Date	Purpose
0	06/07/2015	Document creation
1	27/07/2015	Document revision
2	27/07/2015	Document revision
3	24/09/2015	Document revision
4	16/10/2015	Document approval

DOCUMENT DISTRIBUTION LIST

Name	e-mail
Guillermo Rodríguez	guillermo.rodriguez@alu-etsetb.upc.edu
Montse Nájjar	montse.najar@upc.edu
Mònica Navarro	monica.navarro@cttc.es

Written by:		Reviewed and approved by:		
Date	10/10/2015	Date	16/10/2015	16/10/2015
Name	Guillermo Rodríguez	Name	Montse Nájjar	Mònica Navarro
Position	Project Author	Position	Project Supervisor	Project Co-supervisor

Table of contents

Abstract	1
Resum	2
Resumen	3
Acknowledgements	4
Revision history and approval record.....	5
Table of contents	6
List of Figures	8
List of Tables	10
1. Introduction.....	11
1.1. Work plan	11
1.1.1. Work breakdown structure.....	11
1.1.2. Work packages.....	12
1.1.3. Milestones	15
2. State of the art of the technology used or applied in this thesis:.....	16
2.1. UWB technology.....	16
2.2. IR-UWB for non-invasive estimation of respiration rates	16
3. Methodology / project development:	18
3.1. Model	18
3.1.1. Notation.....	18
3.1.2. Mathematical Model	18
3.2. Respiratory rate detection.....	20
3.2.1. Spectral techniques	21
3.2.2. AR modelling and linear predictor.....	22
4. Results	28
4.1. Simulations.....	28
4.1.1. UWB channel modelling	28
4.1.2. Spectral techniques results.....	32
4.1.3. AR modelling.....	34
4.1.4. Monte-Carlo simulations.....	42
4.2. Experimental results	45
4.2.1. Equipment description	45
4.2.2. Experiment setup	46
4.2.3. Anechoic chamber results	47



4.2.4. Laboratory results.....	50
5. Budget.....	56
6. Conclusions and future development:.....	57
Bibliography:.....	58
Appendices (optional):.....	60
DFT calculation of the clutter removed signal:	60

List of Figures

Fig 1: Slow time and fast time axis representation over $N_s=4$ captured waveforms (considering $p[n] = \delta[n]$) with an oscillating delay progressing along the slow time of the multipath echo corresponding to the chest reflection.	19
Fig 2: AR scheme	22
Fig 3: Linear Predictor scheme	23
Fig 4: AR Scheme	24
Fig 5: Saleh-Valenzuela power delay profile distribution	29
Fig 6: Example of a single channel realization	29
Fig 7: Channel implementation process.....	30
Fig 8: PulsOn 410 series Pulse.....	30
Fig 9: Heatmap of the received signal in the \underline{Y} matrix	31
Fig 10: Heatmap of the received signal once the clutter is removed	32
Fig 11: Bartlett estimation	33
Fig 12: Averaged Bartlett estimation	34
Fig 13: Different Bartlett estimations around the optimal index	34
fig 14: AR power spectral density estimation	35
Fig 15: Frequency estimation evolution over the iterations of the algorithm (zeroes initialization).....	36
Fig 16: Predicted signal, in front of signal to predict over the iterations of the algorithm (zeroes initialization)	36
Fig 17: Prediction error evolution over the iterations of the algorithm (zeroes initialization)	37
Fig 18: Final spectral density estimation with LMS approach (zeroes initialization).....	37
Fig 19: Spectral density estimation of the initialization block with 15 samples.....	38
Fig 20: Frequency estimation evolution over the iterations of the algorithm (block initialization).....	38
Fig 21: Predicted signal, in front of signal to predict over the iterations of the algorithm (block initialization)	38
Fig 22: Frequency shifted signal. Frequency estimation evolution over the iterations of the algorithm (block initialization).....	40
Fig 23: Frequency shifted signal. Predicted signal, in front of signal to predict over the iterations of the algorithm (block initialization).....	40
Fig 24: Frequency shifted signal. Frequency estimation evolution over the iterations of the algorithm (block initialization and increased coefficients, table 11).....	41
Fig 25: Frequency shifted signal. Frequency estimation evolution over the iterations of the algorithm (block initialization and increased update step, table 12).....	41

Fig 26: Root Mean Squared Error of the estimation, Bartlett Estimator	43
Fig 27: Root Mean Squared Error of the estimation, AR block processing	44
Fig 28: Root Mean Squared Error of the estimation, AR LMS	44
Fig 29: Averaged Estimated Frequency of all three estimators	45
Fig 30: Averaged Estimated Frequency of all three estimators (close-up of the last 5 dBs)	45
Fig 31: PulsON 410 MRM with both antennas connected	46
Fig 32: Device setup in anechoic chamber	47
Fig 33: Scheme of the measurement set up	47
Fig 34: Raw data heatmap, anechoic chamber	48
Fig 35: Clutter removal heatmap, anechoic chamber	48
Fig 36: Averaged Bartlett estimation, anechoic chamber	49
Fig 37: AR Power Spectral Density estimation, anechoic chamber	49
Fig 38: Raw data heatmap, laboratory	50
Fig 39: Clutter removal signal, laboratory.....	50
Fig 40: Averaged Bartlett estimation, laboratory	51
Fig 41: AR power spectral density estimation, laboratory.....	52
Fig 42: Frequency estimation evolution of LMS algorithm, laboratory	53
Fig 43: Signal to predict in comparison with predicted signal, laboratory.....	53
Fig 44: Frequency estimation evolution of LMS algorithm, laboratory	54
Fig 45: Signal to predict in comparison with predicted signal, laboratory.....	54
Fig 46: Frequency estimation evolution of LMS algorithm, laboratory	55
Fig 47: Signal to predict in comparison with predicted signal, laboratory.....	55

List of Tables

Table 1: Comparison between AR technique and FFT-Periodogram approach.....	25
Table 2: Comparison between LMS and Block processing coefficient derivation	26
Table 3: Pulse characteristics	31
Table 4: Channel implementation example parameters	31
Table 5: Bartlett estimation parameters	33
Table 6: Averaged Bartlett Estimation parameters.....	33
Table 7: AR Power Spectral Density Estimation parameters.....	35
Table 8: LMS with zeroes initialization parameters	36
Table 9: LMS with block initialization parameters.....	38
Table 10: LMS with frequency shifted signal parameters	39
Table 11: LMS with frequency shifted signal and increased coefficients parameters	40
Table 12: LMS with frequency shifted signal and increased update step parameters.....	41
Table 13: Montecarlo simulations parameters.....	42
Table 14: Averaged Bartlett estimation parameters, anechoic chamber.....	48
Table 15: AR Power Spectral Density estimation parameters, anechoic chamber	49
Table 16: Averaged Bartlett estimation parameters, laboratory.....	51
Table 17: AR power spectral density estimation parameters, laboratory	52
Table 18: LMS parameters, laboratory.....	52
Table 19: LMS algorithm setup for respiratory patterns (apnoea) detection parameters, laboratory	54
Table 20: LMS algorithm setup for respiratory patterns (shortness of breath associated to tachycardia) detection parameters, laboratory	55

1. Introduction

The respiratory frequency monitoring has many uses and applications related to the medical field. Some of them are respiratory rate tracking during sleep studies or chronic obstructive pulmonary disease (COPD) diagnosis, sudden infant death syndrome (SIDS) detection in preterm infants or patient vital signs overseeing in hospitals or residences. Also, outside of a strict medical environment, the need for sensor system solutions for home monitoring is growing as the life expectancy of the world population is increasing [1]. Possible targets for this home monitoring are elderly, disabled or chronically ill people.

Besides tracking the respiratory rate in a quantitative way, we could detect irregularities in that steady frequency, referred as respiratory patterns. One concrete case of a respiratory pattern is the apnoea episode. An apnoea is defined as “an unexplained episode of cessation of breathing for 20 seconds or longer, or a shorter respiratory pause associated with bradycardia, cyanosis, pallor, and/or marked hypotonia[2]”. The appearing of apnoea episodes in critical situations like post-operative [3] or preterm birth [4] can imply severe risks and complications. And even in its most common appearance as sleep apnoea, the actual practices to monitor those episodes still entail expensive and uncomfortable overnight stays at healthcare centres.

Taking all of that into account, the demand of non-invasive, flexible (able to take measurements in any scenario), real-time and cost effective solutions to perform vital sign monitoring, and more concretely, respiratory frequency, arises.

Following that need, the main goal of this thesis is to develop a Wireless system able to accomplish the following objectives:

- Monitor the respiratory rate of a patient.
- Monitor and detect respiratory patterns like apnoea or breathe shortness associated with tachycardia episodes.

In this thesis we develop, from one part, all the corresponding signal processing and from the other, all the interaction and configuration the used UWB hardware device, which is in charge of doing the UWB sensing and return the raw data to be processed.

1.1. Work plan

As in previous documents, we are going to organize the work in a system based on tasks, milestones and a Gantt diagram (which is placed at the appendices).

1.1.1. **Work breakdown structure**

1. HW and API interaction
 - 1.1. First contact with example software
 - 1.2. Connect the HW to Matlab
 - 1.3. Test simple measurements
 - 1.4. Prepare and obtain data in different scenarios
 - 1.5. Final HW adjustment
2. Software simulation
 - 2.1. Obtain and evaluate channel model
 - 2.2. Adapt channel to our situation
 - 2.3. Reproduce a “basic” breath detecting system
3. Signal processing to obtain breath rate

- 3.1. Remove the clutter of the signal
- 3.2. Try different algorithms and transformations
- 4. Apnea detection
 - 4.1. LMS Algorithm implementation
 - 4.2. Adjust LMS algorithm to detect a steady breath rate
 - 4.3. Adjust LMS algorithm to detect a varying breath rate (i.e. apnea episode)
 - 4.4. Final data acquisitions

1.1.2. Work packages

Project: UWB for Medial Apps	WP ref: WP1	
Major constituent: HW and API interaction		
Short description: Comprehend the HW and be able to obtain the desired data from it.	Start date: 09-03-2015 End date: 13-09-2015	
	Start event: First contact with the device. End event: Obtain fully consistent data for further processing.	
Internal task T1: First contact with example software. Analyze the given example software to understand the basic behavior of the technology and the HW. The example software can be found in the manufacturer's site, addressed to developers who want to build applications with its devices. Internal task T2: Connect the HW to Matlab. Time Domain supplies a C and Matlab APIs to ease the integration with computers or with other microprocessors. Internal task T3: Test simple measurements. Build a script able to obtain the raw data directly from the device ready for its processing. Internal task T4: Prepare and obtain data in different scenarios. Produce some measurements with human target in two situations. First, in the anechoic chamber, to obtain a clearer signal and second, in a standard scenario with multipath reflections	Deliverables:	Dates:

<p>Internal task T5: Readjust the device to set the sampling frequency to the expected one by adjusting our software and doing the pertinent calls to the API of the HW. Some issues related to the Matlab intrinsic delays were solved.</p>		
--	--	--

<p>Project: UWB for Medial Apps</p>	<p>WP ref: WP2</p>	
<p>Major constituent: Software simulation</p>		
<p>Short description:</p> <p>Reproduce and simulate the work environment and breath detection system</p>	<p>Start date: 10-04-2015 End date: 20-05-2015</p> <p>Start event: Obtain channel model scripts End event: Obtain fully coherent and reliable simulation data to test the algorithms with them.</p>	
<p>Internal task T1: Obtain and evaluate channel model. Investigate the concrete features of the UWB propagation channel, find its differences in front of a typical narrowband environment. And finally, look for or implement the required channel in the Matlab software.</p> <p>Internal task T2: Adapt channel to our situation. Once we have the impulse response of an indoor UWB propagation channel, we modify it to add the multipath echoes related to the chest of a human being.</p> <p>Internal task T3: Reproduce a “basic” breath detecting system. Implement the breath detection system that most of the found papers propose as basic structure. Those systems are based in three stages: Simulate (or use of real data if they have it) the radar signal, clutter removal (almost always subtracting an average of the received signal) and a transformation (like FFT) approach to obtain the breath frequency.</p>	<p>Deliverables:</p>	<p>Dates:</p>

Project: UWB for Medial Apps	WP ref: WP3	
Major constituent: Signal processing to obtain breath rate		
Short description:	Start date: 06-04-2015 End date: 17-05-2015	
Signal processing to extract breath rate information of the stored data	Start event: Clutter removal process. End event: Count with a set of different signal processing approaches to detect the breath rate.	
Internal task T1: Pre-process the data to remove the clutter of the signal. We try different techniques to extract the static reflections of the obtained data related to multipath reflection of steady objects in the scenario. This allows an easier processing of the useful signals. Internal task T2: Try different algorithms and transformations to obtain the breath signal. Possible transformations could be: Based on spectral techniques (like FFT, Periodogram, Bartlett estimator), Based on AR modeling (with different approaches to estimate the optimal coefficients). Report advantages and drawbacks of each solution and chose the optimal one.	Deliverables:	Dates:

Project: UWB for Medial Apps	WP ref: WP4	
Major constituent: Apnea / Respiratory patterns detection		
Short description:	Start date: 28-05-2015 End date: 20-09-2015	
Apnea is defined as the suspension of external breathing. We are able to detect it when the inhalation movement that we are monitoring is stopped. Also, we are able to detect different respiratory patterns, like the breath shortness associated with tachycardia episodes.	Start event: LMS Algorithm purpose approach. End event: Fully working system.	

<p>Internal task T1: LMS Algorithm implementation. Design and implement a solution based in the Least Mean Square adaptive algorithm. Test the first implementation with simulation data.</p> <p>Internal task T2: Adjust LMS algorithm to detect a steady breath rate. Tweak the parameters and configurations of the algorithm to make it able to detect a steady breath signal extracted from real data from the experiments.</p> <p>Internal task T3: Adjust LMS algorithm to detect a varying breath rate (i.e. apnea episode). Tweak the parameters and configurations of the algorithm, but this time with the objective of balancing the trade-offs of the response to make it able to detect rapid transitions in the signals. The signal is extracted again from real data from the experiments.</p> <p>Internal task T4: Final data acquisitions and tests. Final data acquisitions with all the appropriate configurations. Controlled breath rate transitions allow us to obtain proper data to do the final analysis.</p>	<p>Deliverables:</p>	<p>Dates:</p>
---	----------------------	---------------

1.1.3. Milestones

WP#	Task#	Short title	Milestone / deliverable	Date (week)
1	4	Obtain first valid working data	First working data	9 th week
2	3	Obtain basic breath detecting system	Properly working software	10 th week
3	2	Chose optimal signal processing	Breath rate measurement	11 th week
4	3	Obtain fully working system to detect apnea / respiratory patterns	Apnea / Respiratory patterns detection application	20 th week

2. State of the art of the technology used or applied in this thesis:

Available solutions in common medical practice include solutions like the impedance pneumography [5] and thoraco-abdominal bands and following with tools as inductive plethysmography, thermistors and thermocouples, nasal prongs, etc [6]. But the main drawback of those techniques is that there is always a wired physical sensor touching the skin of the patient in some way, and if we want the system to operate in the least invasive way we need to avoid those approaches.

Systems for remote respiratory rate tracking have also emerged in the last years. Some of them are based on Doppler radar techniques [7]. However, Doppler radar techniques present some problems, like the difficulty they have in penetrating material, among other difficulties [8]. Another case of strictly non-touching technique is the functional magnetic resonance imaging (fMRI). This method is actually providing images of moving internal organs without physical contact but, as it uses induced field, the patient has to be confined in space; while UWB or WiFi solutions, using radiated field, lets the patient be absolutely free in space.[10]

2.1. UWB technology

To overcome those problems in the wireless sensing the Ultra-wide Band (UWB) technology is presented. Impulse Radio (IR) UWB wireless systems are generally based on the transmission and reception of sub-nanosecond pulses without carriers or modulated short pulses with carriers. The extremely wide bandwidth generated by this technique allows UWB systems to have a set of distinct characteristics that make them very suitable for biomedical applications. Some of those features are that it radiates and consumes little power, coexists well with other instruments, and is robust to interference and multipath. Besides that, accomplishing with the proposed requirements, it is claimed that such wireless systems can provide low system complexity, low cost and low power consumption [9].

Multipath resolution down to a fraction of a nanosecond provides excellent spatial resolution for short range radar applications in addition to being able to resolve and deal with significant multipath fading. The use of IR-UWB signals has been suggested for several medical applications because of the high spatial resolution provided by these signals [10].

2.2. IR-UWB for non-invasive estimation of respiration rates

As a matter of fact, radar monitoring of human physiologic functions was considered as early as the 70's, but any further development was impeded by the inconvenience and expensive technology of those times [10].

Now that the technology has sufficiently evolved, this thesis presents a system able to estimate and track the breathing rate using an UWB Radar in real time. Given the mentioned precise spatial resolution, the basic principle of this measurement relies on tracking the chest oscillation of the patient (in the order of few cm) due to the breathing process, and with it, detect the respiratory frequency. The fact that the coefficient of reflectivity of air-to-dry-skin interface for electromagnetic waves in the 300-900MHz range is about 72% [10] eases measuring that signal.

Following the proposed approach different authors have presented their solutions to estimate the breathing rate [9], [11], [20], [21] and [22]. From those sources, each author present different innovations: mathematical frameworks to analyse the harmonic contributions in the breath signal measurement, estimation of the amplitude of chest movement, theoretical estimation limits, etc. But all the proposed measuring and frequency techniques consider no variation in the breathing rate while using UWB. None of the mentioned solutions is focused on an adaptive solution, as the one that we are presenting in this thesis to address the apnoea problem in a real time regime. Nevertheless, there exist wireless solutions to detect apnoea episodes based on Doppler radar but they lead to poor characteristics in the response compared to the UWB approach.

3. Methodology / project development:

3.1. Model

The theoretical model considered in this work is based on [11] and [9] approaches. With this model we establish a mathematical framework so that the spectrum of the received signal can be obtained and understood.

3.1.1. Notation

To fully describe the sampling process of the received waveforms in the radar we use two time axis. The first time-axis is associated to the range along each received waveform and is denoted as "fast-time" (τ). The sampling period in the fast time-axis T_f has the order of nanoseconds.

The second time-axis regards the measurement between successive received full waveforms and is referred to as "slow-time" (t). The sampling period in this case T_s is of the order of seconds.

The received waveforms at the radar device are measured at discrete instants in the slow time $t = nT_s$ with $n = 1, 2, \dots, N_s$. Regarding the fast time, each single waveform is measured at sampling period T_f , resulting in the discrete instants $= mT_f$ with $m = 1, 2, \dots, N_f$.

3.1.2. Mathematical Model

The subject chest nominal distance d_0 is defined as the distance between the radar device and the person to be monitored. However, due to respiration, the chest cavity expands and contracts periodically (in a normal regime), and so the distance travelled by the corresponding multipath component $d_l[n]$ also varies periodically around the nominal distance as follows:

$$d_l[n] = d_0 + g[n] \quad (1)$$

Assuming the variation in the lung and chest movement as a sinusoidal function of time as in [9] and [11] with a normalized respiration rate $f_b = \frac{f_{\text{respiration rate}}}{f_{\text{slow-time sampling}}}$ we can reformulate equation (1) as:

$$d_l[n] = d_0 + g[n] = d_0 + \Delta_d \sin 2\pi f_b n \quad (2)$$

where Δ_d represents the maximum deviation of the chest movement. With the assumption that the environment (besides the subject to be monitored) is static, the time-varying channel impulse response $h[n, m]$ is composed of two terms

$$h[n, m] = \underbrace{\sum_i \alpha_i \delta(m - m_i)}_{\text{static channel}} + \underbrace{\alpha_b \delta(m - m_b[n])}_{\text{respiratory variations}} \quad (3)$$

where n and m denote slow and fast time respectively, α_i is the amplitude of each multipath component and m_i its delay, α_b is the amplitude of the multipath component corresponding to the chest of the subject. Also, in the equation (3) $m_b[n]$ is given by:

$$m_b[n] = \frac{d_l[n]}{c} = \frac{d_0 + \Delta_d \sin 2\pi f_b n}{c} = m_0 + m_d \sin 2\pi f_b n \quad (4)$$

where c is the speed of light in vacuum. Neglecting pulse distortion and other non-linear effects, the signal measured by the receiver antenna can be written as the convolution of the transmitted pulse, $p[m]$, and the channel impulse response. Ignoring noise, the received signal $y[n, m]$ measured can be written as:

$$y[n, m] = p[m] * h[n, m] = \sum_i \alpha_i p[m - m_i] + \alpha_b p[m - m_b[n]] \quad (5)$$

At this point we already have a representation of the received signal as the sum of the static responses of the channel together with the variant response due to the chest movement as in the following Figure:

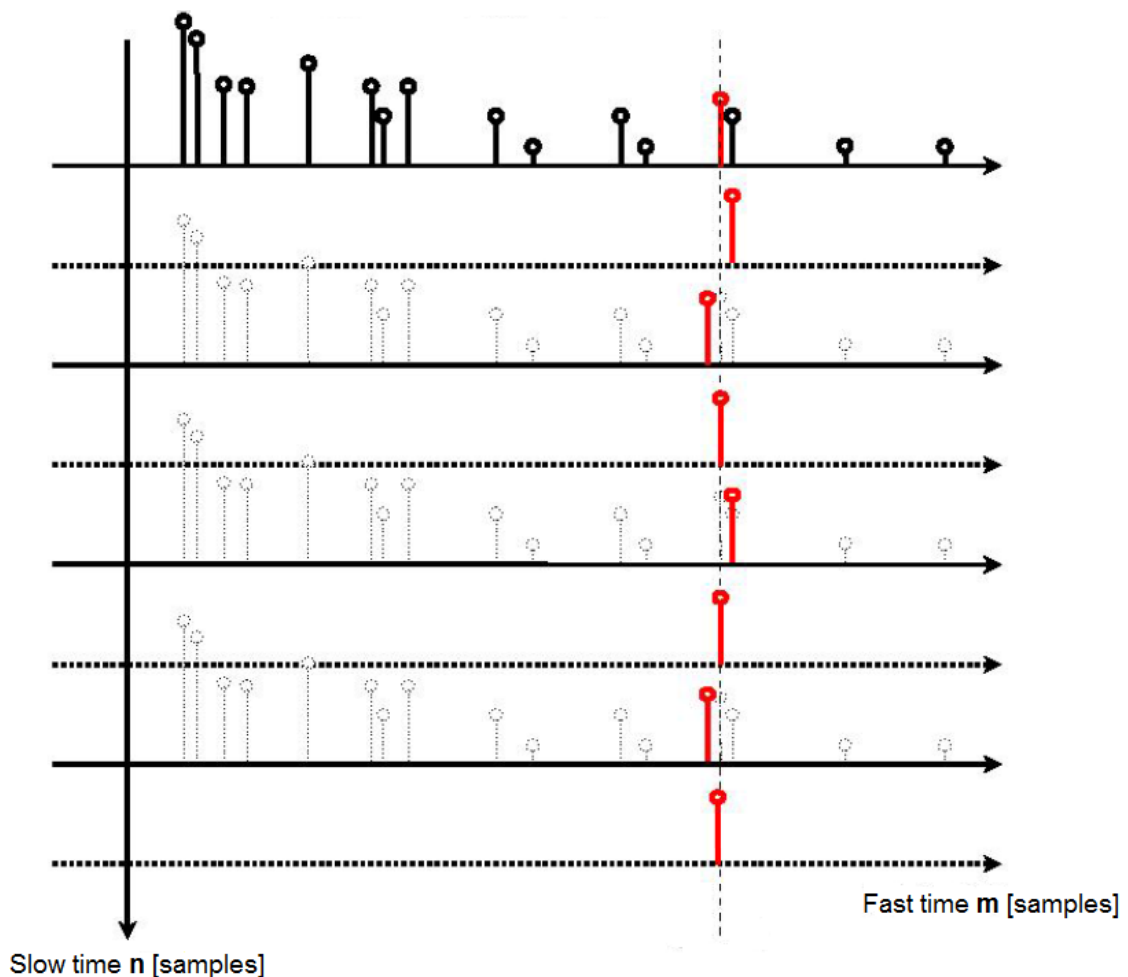


Fig 1: Slow time and fast time axis representation over $N_s=4$ captured waveforms (considering $p[n] = \delta[n]$) with an oscillating delay progressing along the slow time of the multipath echo corresponding to the chest reflection.

As seen in Figure 1, to have a clear distinction between the respiratory variations (red multipath echo) and the static channel, we need to have a waveform alignment in the slow time axis. This alignment pre-processing is omitted in our case, given that the hardware used for the experimental results, that we present later, aligns the samplings automatically.

To better manage this data along these two different time axis we compose the responses matrix $\underline{\underline{Y}}$, the elements of which are:

$$\underline{\underline{Y}} = \{y[n, m]\}, 1 \leq n \leq N_s, 1 \leq m \leq N_f \quad (6)$$

In this way, the i th column of the matrix $\underline{\underline{Y}}$ represents the samples corresponding to the i th received waveform.

3.1.2.1. Clutter removal

As seen in many other radar applications, there is a need of removing static channel responses (background clutter) to better distinguish the relevant moving signals. Assuming in our case of study that the only motion present is the subject's chest movement, thus, our clutter is generated by the stationary scatters in the multipath environment. Since we want separate the moving scatters from the stationary scatters, we need to apply a motion-filter to the data.

An easy approach to solve this problem would be to simply average all the received waveforms and then, subtract this average from each individual response. We are doing nothing more than a high pass filtering, as the average of the signals captures the constant features of the responses.

An implementation of this motion filter would be given by the following expression:

$$x[n, m] = y[n, m] - \frac{1}{N_s} \sum_{i=0}^{N_s-1} y[i, m] \quad (7)$$

Where $y[n, m]$ is the received response and $x[n, m]$ is the clutter removed signal. If from equation (5) we further develop this expression, it leads to:

$$x[n, m] = \alpha_b p[m - m_b[n]] - \underbrace{\frac{1}{N_s} \sum_{i=0}^{N_s-1} \alpha_b p[m - m_b[i]]}_{x_0(m)} \quad (8)$$

In equation (8) the multipath echo of interest is isolated from a residual subtracting element $x_0(m)$, where $x_0(m)$ is the averaged signal over the slow time axis corresponding to the chest movement multipath.

3.2. Respiratory rate detection

The main technique we have considered to track the respiratory rate of the subject is based on frequency analysis applied to the received signal in the radar device. In the current section we are going to propose different frequency estimators that allow us to visualize and obtain that information through different approaches.

In spite of the fact that there are numerous frequency estimation schemes in the literature, they can be generally classified as nonparametric or parametric approaches. The nonparametric frequency estimators, including the Periodogram and its variants, are

obtained directly from the Fourier transform of the received signal. Although no assumptions are made about the observed data sequence, the resolution, or ability to resolve closely spaced frequencies using the nonparametric approach is fundamentally limited by the length of the data available (number of samples used in the Fourier transform calculation). Alternatively, the parametric approach, which assumes that the signal satisfies a generating model with known functional form, can attain a higher resolution [12].

3.2.1. Spectral techniques

Starting with a nonparametric estimation of the spectral density of the signal, we implement a solution based on the Bartlett's Method. Bartlett's method (also known as the method of averaged periodograms) is an improvement on the standard periodogram spectrum estimating method, as it reduces the variation in the estimated power spectra in exchange of reducing the frequency resolution [13]. An estimate of the spectrum using this technique is obtained by averaging the estimates from the periodograms derived from a non-overlapping portions of the original signal.

Considering K segments of L samples, and consequently with the length of the signal $N = K \times L$, the following equation corresponds to the Bartlett power spectral estimator of the clutter removed signal from equation (8):

$$\hat{S}_B[k, m] = \frac{1}{N} \sum_{i=0}^{K-1} \underbrace{\left| \sum_{n=0}^{L-1} x[n + iL, m] e^{-\frac{j2\pi kn}{L}} \right|^2}_{\text{Periodogram}} \quad (9)$$

So, to obtain this spectral representation, first we have to calculate the Discrete Fourier Transform (DFT) of the clutter removed signal $x[n, m]$ to then calculate the periodogram (see the appendix for the development).

The spectrum along the slow time of the clutter removed respiratory rate signal is composed by several shifted sinc signals placed at the harmonics of the interest frequency, f_b in this case. Besides of those harmonics, there is an additional coloured noise contribution as result of filtering the AWGN.

Analysing the results, we can state that between all of the resulting sincs, the one with the maximum value can be found at $m = m_0$. Where m_0 corresponds to the fast-time instant where the reflection of the chest movement is found. So, to obtain the respiratory rate frequency we first need to estimate the \hat{m}_0 value.

To obtain \hat{m}_0 we can simply average the output of the motion filter along the slow time index n on equation (8) and choose $m = \hat{m}_0$ that maximizes this average. Taking into account that we have assumed that the only movement in the environment is the chest oscillation, the average of the motion filter output gives us the position of where that movement is.

$$\hat{m}_0 = \max_m \sum_{n=0}^{Ns-1} |x[n, m]|^2 \quad (10)$$

As seen on equation (10) we are only selecting a single optimal fast time index \hat{m}_0 with a broad estimation. But in fact, the chest movement affects more than one fast time index, given that the width of the emitted pulse covers more than a single fast time position. This

leads to a margin around the most relevant index where there is also a considerable amount of information. To take advantage of that margin, we select a range before and after the \hat{m}_0 fast index sample to enhance the spectral estimation.

$$\hat{S}_{averaged}[k] = \frac{1}{2M} \sum_{m=\hat{m}_0-M}^{\hat{m}_0+M} \left(\frac{1}{N} \sum_{i=0}^{K-1} \left| \sum_{n=0}^{L-1} x[n+iL, m] e^{-\frac{j2\pi kn}{L}} \right|^2 \right) \quad (11)$$

Averaging over the Bartlett estimations in the range of $m = \hat{m}_0 \pm M$ we achieve a further noise reduction and smoothing of the harmonic components without losing frequency resolution (as we are not reducing the number of samples).

3.2.2. AR modelling and linear predictor

The Fourier technique for spectral analysis assumes that the signal can be modelled by a sum of sinusoids (or complex exponential functions). Depending on the particular data to be analysed, the Fourier model may not be the best one to describe the process. That means that there might be an alternative model that uses fewer parameters to describe the signal, or perhaps that would not suffer from the detrimental effects of the model mismatch made about the behaviour of the data outside the measured interval [14].

Instead, we can consider a parametric approach with no specific assumptions on the signal waveform but on the linear dependency of the time-varying process. In particular, we focus on the AR model, which assumes that the current value of the process, $x(n)$ can be described by a finite linear composition of the previous values of the process and the current value of a white noise driving the source $w(n)$. An AR process of zero mean and order p is defined as:

$$x(n) = w(n) - a_1x(n-1) - a_2x(n-2) - a_3x(n-3) \dots - a_px(n-p) \quad (12)$$

The AR model contains $p + 1$ parameters which have to be estimated from the data: the AR coefficients $\{a_i\}$ with $i = 1, 2, \dots, p$ and the variance of the white noise σ^2 .

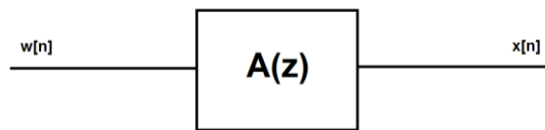


Fig 2: AR scheme

Once we estimate the parameters, both a_i and σ^2 , the AR Power Spectral Density Estimation of the data is given by:

$$S(k) = \frac{\sigma^2}{\left| \sum_{i=0}^p a_i e^{-j2\pi ik} \right|} \quad (13)$$

Where $a_0 = 1$

There are several methods to estimate those coefficients. In the following sections we present two different approaches. Each method is going to provide us different trade-offs of features, with its advantages and drawbacks.

A common way to define the coefficients is through a Linear Predictor. A Linear Predictor is a system able to predict future values of a target signal based on its past values. At the output of the Linear Predictor we obtain the prediction error, which is the difference between the prediction and the signal to predict. Ideally, this error is white noise.

Here we present the structure of a linear predictor of p coefficients:

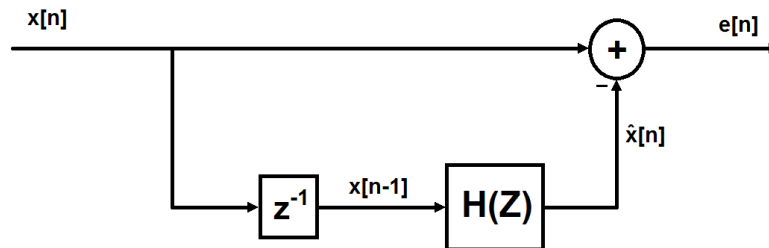


Fig 3: Linear Predictor scheme

With $x[n]$ signal to predict, $\hat{x}[n]$ the predicted signal, $e[n]$ the prediction error defined as:

$$e[n] \triangleq x[n] - \hat{x}[n] = x[n] - \underline{h}^H[n] \underline{x}[n-1] \quad (14)$$

With:

$$\underline{x}[n-1] = [x[n-1] \ x[n-2] \ \dots \ x[n-p]]^T \quad (15)$$

And the coefficients vector \underline{h} :

$$\underline{h} = \begin{bmatrix} h_1 \\ \vdots \\ h_p \end{bmatrix} \quad (16)$$

To compose a linear predictor of this kind we need to find out the value of the p optimal coefficients of \underline{h} . A common solution is the minimum mean squared error (MMSE) [ref] at the output of the predictor following the equation:

$$\underline{h}_{\text{MMSE}} = \underset{\underline{h}}{\text{arg min}} E\{|e[n]|^2\} \quad (17)$$

3.2.2.1. Block processing coefficients

The first approach to find the AR coefficients is to apply a block processing with the well know Wiener optimal filter solution [19]:

$$\underline{h} = -\underline{\underline{R}}^{-1} \underline{r} \quad (18)$$

where:

$$\underline{\underline{R}} = E\{\underline{x}[n] \underline{x}[n]^T\} \quad (19)$$

$$\underline{x}[n] = [x[n] \ x[n-1] \ \dots \ x[n-p-1]]^T \quad (20)$$

$$\underline{r} = E\{x[n]\underline{x}[n-1]\} \quad (21)$$

and \underline{R}^{-1} denotes matrix inversion.

If we now, invert the AR system proposed in Figure 2 we obtain the following structure:

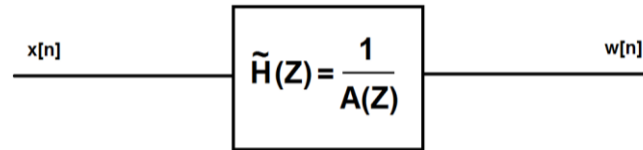


Fig 4: AR Scheme

Which resembles the one presented in Figure 3, corresponding to the Linear Predictor, given that both systems are whitening the output signal. We can compose the new vector coefficients of the inverted AR model as:

$$\underline{\tilde{h}} = \begin{bmatrix} 1 \\ -h_1 \\ \vdots \\ -h_p \end{bmatrix} \quad (22)$$

Which fulfils equation (14) with a more compact expression of the error at the output of the system following:

$$e[n] = x[n] - \underline{h}^H[n]\underline{x}[n-1] = \underline{\tilde{h}}^H \underline{\tilde{x}}[n] \quad (23)$$

Where:

$$\underline{\tilde{x}}[n] = [x[n] \ x[n-1] \ \dots \ x[n-p]]^T \quad (24)$$

With the estimated coefficients, we can proceed to calculate the power spectral density estimate using equation (11). From there we find the maximum peak value in the estimated spectrum, which abscises-index corresponds to the estimated respiratory frequency.

AR technique	FFT-periodogram
<ul style="list-style-type: none"> - Better stability for short segments of signal - Better spectral resolution (less dependent on the record length) - Better temporal resolution 	<ul style="list-style-type: none"> - FFT is widely available and is the first-line engineering approach towards spectral analysis - Shorter processing time (about four times faster in the FFT-periodogram)

	<ul style="list-style-type: none"> – Slightly easier to code – Less sensitive to numerical round-off errors – Does not depend in model order choices
--	---

Table 1: Comparison between AR technique and FFT-Periodogram approach

3.2.2.2. Adaptive coefficients

As seen in the previous section, the coefficients of the AR filter can be obtained through the Wiener Filter solution. To be able to apply that method, second order statistics of the signal are required. However, those statistics are not always available. A case under those restrictions is the real-time or online processing. More specifically, in the scenario of interest we need to detect changes in the respiratory frequency (respiratory patterns like apnoea), where the signal arrives sample by sample. A common alternative to solve this type of problems is the use of adaptive filters.

Such filters start from initial conditions that can contain no desired information and then update their filter weights based on a sequence of input data. For stationary inputs, it has been shown that with a proper algorithm, the mean weight vector of adaptive prediction error filters converges to the optimal AR coefficients [15].

One of the most commonly used algorithms is the least-mean-square (LMS). Being this algorithm one of the most simple yet effective in real applications.

The idea behind the LMS filter is to use the steepest descent to approach the optimum filter weights updating them step by step, in a direction given by the MSE gradient. So, the basic weight update equation considering the complex case (as a generic demonstration) is:

$$\hat{\underline{h}}[n+1] = \hat{\underline{h}}[n] - \underbrace{\mu \nabla_{\hat{\underline{h}}^H} E\{|e[n]|^2\}}_{MSE\ gradient} \quad (25)$$

Being $\hat{\underline{h}}$ the estimation of the coefficients vector. Also, μ is the update step and $e[n]$ is defined as the prediction error in the current instant n as in equation (14).

The negative sign in the factor that modifies the filter weights indicates that, we need to change the weights in a direction opposite to that of the gradient slope to readjust the approaching direction. In that way our filter progress towards the minimum error of prediction.

To derive the final LMS expression first, we develop the MSE gradient factor in (43):

$$\nabla_{\hat{\underline{h}}^H} E\{|e[n]|^2\} = \nabla_{\hat{\underline{h}}^H} E\{e[n]e^*[n]\} = E\{\nabla_{\hat{\underline{h}}^H}(e[n]e^*[n])\} \quad (26)$$

With:

$$\nabla_{\hat{\underline{h}}^H} E\{e[n]\} = \nabla_{\hat{\underline{h}}^H} (x[n] - \hat{\underline{h}}^H \underline{x}[n-1]) = -\underline{x}[n-1] \quad (27)$$

By replacing (45) in (44) yields,

$$\nabla_{\hat{\underline{h}}^H} E\{|e[n]|^2\} = -E\{\underline{x}[n-1]e^*[n]\} \quad (28)$$

Finally, applying (46) to (43) we obtain:

$$\hat{\underline{h}}[n+1] = \hat{\underline{h}}[n] - \mu \nabla_{\hat{\underline{h}}^H} E\{|e[n]|^2\} = \hat{\underline{h}}[n] + \mu E\{\underline{x}[n-1]e^*[n]\} \quad (29)$$

This is a valid expression of an adaptive algorithm, but, to allow a real-time LMS updating we cannot afford doing the expectation with all the samples. Instead, we use an instantaneous estimate of the expectation. Using the unbiased estimator:

$$E\{\underline{x}[n-1]e^*[n]\} = \frac{1}{N} \sum_{i=0}^{N-1} \underline{x}[n-1]e^*[n-i] \quad (30)$$

And selecting a single sample in (48) with $N = 1$:

$$E\{\underline{x}[n-1]e^*[n]\} = \underline{x}[n-1]e^*[n] \quad (31)$$

We obtain the final formula introducing (49) in (47):

$$\hat{\underline{h}}[n+1] = \hat{\underline{h}}[n] - \mu \underline{x}[n-1]e^*[n] \quad (32)$$

In this way, as we receive each sample from the radar device we are able to update the filter using the previous equation, since it only depends on a new sample of the interest signal.

As in the previous section, we reintroduce the parameters in equation (13) composing a new vector of coefficients as in equation (22).

With that, we obtain the power spectral density estimation of the desired signal at each update over the filter coefficients. In that way we are able to track the progression in the respiratory frequency of the patient if there is any variation in it (like apnoea episodes).

LMS	Block processing
<ul style="list-style-type: none"> - Adaptive response - Better time resolution - Less computational cost 	<ul style="list-style-type: none"> - More precise - No stability problems - The only parameter that we need to define is the number of coefficients

Table 2: Comparison between LMS and Block processing coefficient derivation

3.2.2.2.1. Convergence of the LMS algorithm

As the LMS does not use the exact values of expectations using this approach will not reach the optimum value, but it can converge in terms of its mean value. Even if the updates

on the algorithm are small, there will always be a dispersion over the optimal value related with the update step. Moreover, if the step in each iteration is too large the system may not even converge and turn out unstable.

To control the evolution of this adaptive system we have to adjust the update step μ . About this constant, it can be proved [16] that its value is bounded by:

$$0 < \mu < \frac{2}{\lambda_{max}} \quad (33)$$

Where λ_{MAX} corresponds to the largest eigenvalue of the autocorrelation matrix of the signal. If this condition is not fulfilled, the system do not converges and the algorithm turns out unstable.

But, we have to take into account that the autocorrelation matrix of the signal may not be available, so instead, we can use the following more restrictive condition:

$$0 < \mu < \frac{2}{\mathbf{pr}_x(\mathbf{0})} < \frac{2}{\lambda_{max}} \quad (34)$$

since

$$\lambda_{max} < \sum_i \lambda_i = \text{tr}(\underline{\underline{R}}) \quad (35)$$

Given that $\underline{\underline{R}}$ is the $p \times p$ autocorrelation matrix of the signal the trace satisfies:

$$\text{tr}(\underline{\underline{R}}) = p r_x(0) \quad (36)$$

4. Results

This section provides numerical evaluation of the proposed method by means of simulations and experimental measurements.

4.1. Simulations

For the assessment of the respiratory tracking scheme and apnoea detection we have first to evaluate a simulated scenario, a situation where a patient breathes steadily for a specific time interval. To do so, first we introduce the channel model we have considered for the operation of the UWB radar system. Then, we apply the proposed solutions to estimate the respiratory rate frequency in illustrative particular cases. Starting with analysis by Spectral Techniques (Periodogram-based solutions in this case) and following with AR modelling. Inside the AR modelling, we first obtain the coefficients of the AR model with block processing calculation and then, apply the LMS filter. Inside the LMS simulations, we modify the parameters of the model to emulate variations in the respiratory rate, and with it, test the response of our wireless system to those situations. Finally, we implement a series of Monte-Carlo simulations over our different solutions to evaluate its performance.

4.1.1. **UWB channel modelling**

The channel model specifies the channel impulse response in equation (3). First, we introduce the channel impulse response in the static regime (static channel) and then we add the respiratory variations modelling.

4.1.1.1. **Static channel**

To obtain a set of simulations that are as close as possible to the real working environment we developed our own scripts on top of a reliable channel model.

To do so, after reviewing different literature about the UWB channel modelling, we finally used the model proposed by the research group IEEE 802.15.4a [23]. This is a widely recognised model for UWB channels, and additionally, they provide a set of Matlab scripts for its implementation. Those scripts provide models for several types of channels, and among them, different UWB environments in the range from 2 to 10 GHz for different situations. To summarize the key features of the model we highlight:

- model treats only channel, while antenna effects are to be modelled separately
- d^{-n} law for the path loss
- frequency dependence of the path loss
- modified Saleh-Valenzuela model:
 - arrival of paths in clusters of rays instead of single rays.
 - mixed Poisson distribution for ray arrival times
 - possible delay dependence of cluster decay times
 - the power delay profile is composed accordingly to LOS or NLOS conditions (i.e. in some NLOS environments the multipath component with higher amplitude is not the first arriving reflection)

- Nakagami-distribution of small-scale fading, with different m-factors for different components
- block fading: channel stays constant over data burst duration

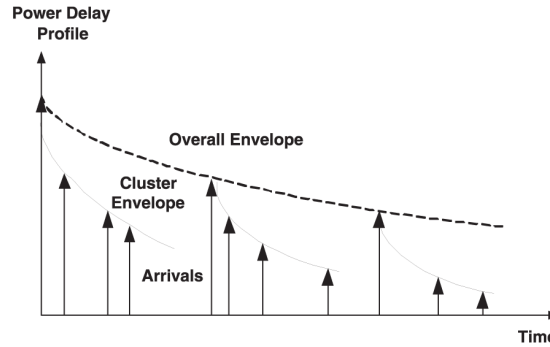


Fig 5: Saleh-Valenzuela power delay profile distribution

The structure of the Saleh-Valenzuela model in which the UWB channel modelling is based can be explained from a physical viewpoint. The rays within a cluster are formed by multiple reflections from objects in the vicinities of the transmitter and the receiver (e.g., room walls, furnishings, and people). This is because of the high time domain precision of the UWB signal. Due to this resolution, instead of receive a single multipath echo from an object in the environment, we receive a cluster corresponding to the different edges or shapes of that object.

Given all the mentioned characteristics, the shape of a single channel realization looks like the following:

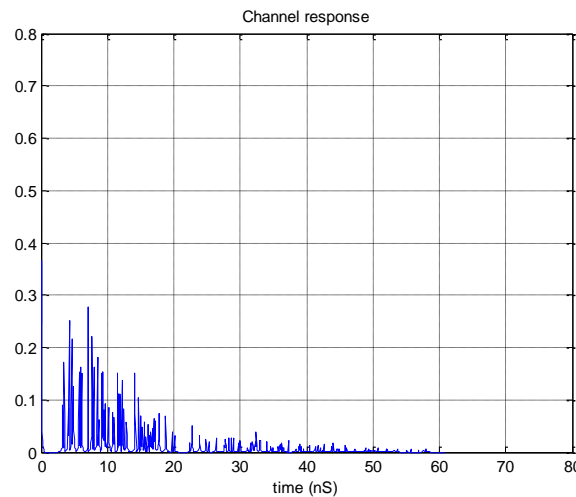


Fig 6: Example of a single channel realization

4.1.1.2. Respiratory variations

At this point we consider the implementation of a single simulation of a patient breathing in a static environment to illustrate the aspects of the simulation set-up and model. This simulation is composed by N_s captured waveforms with a slow time sampling frequency F_s . Considering a short enough total measuring time and the steadiness assumption of the

channel we can assume that the static channel maintains its shape along all the captured waveforms.

Taking that assumption into account, we generate the channel pulse response as in equation (3) in the structure of the following scheme in Figure 7:

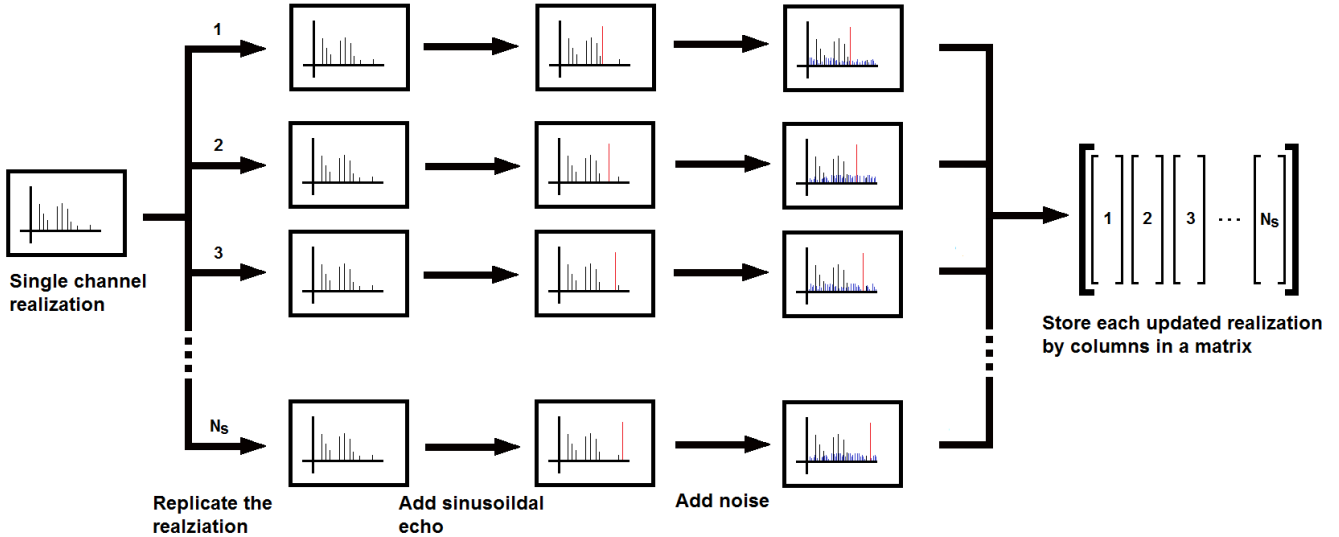


Fig 7: Channel implementation process

In this process, we select a single static channel realization following the UWB channel modelling description in the past section. Then, we replicate it across the N_s slow time samplings. Following that, we add an additional multipath echo in each repetition of the static channel with a variant position over the fast time index m . The position of that echo depends on the slow time index n following equation (4). Additionally, we add the AWGN noise contribution neglected in the first part of the theoretical approach.

Now that we have the channel response, we have to populate the matrix Y from equation (6). To do so, we convolve each channel impulse response with the pulse emitted by our UWB radar device.

The shape and features of our simulated pulse are constrained by the real characteristics of the pulse generated by our HW device. From the documentation of the PulsOn 410 series we obtain the following plot:

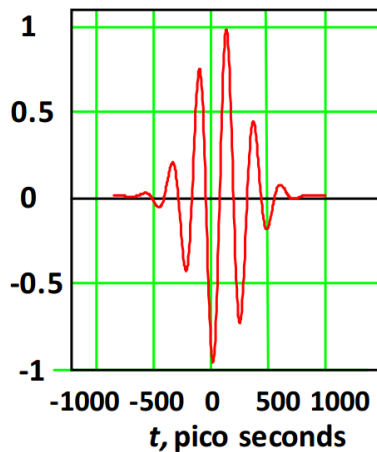


Fig 8: PulsOn 410 series Pulse

Which corresponds to a Gaussian pulse of central frequency 4.3GHz. To model it, we use the Matlab function *gauspuls*[24] with the following characteristics:

Central Frequency	4.3GHz
Fractional Bandwidth	60%
Fractional Bandwidth Reference Level	-40dB

Table 3: Pulse characteristics

Now, we chose a set of parameters to compose an example of the presented implementation of a patient breathing in a static environment.

N_s	1000
f_s	10Hz
f_b	0.24Hz
m_d	0.025m
m_0	2m
SNR	0dB

Table 4: Channel implementation example parameters

The parameters in Table 4 are compliant with real typical values as suggested in [9] With those parameters we populate and represent in a heat map the $\underline{\underline{Y}}$ matrix, or in other words, our simulated received signal. We obtain the following results:

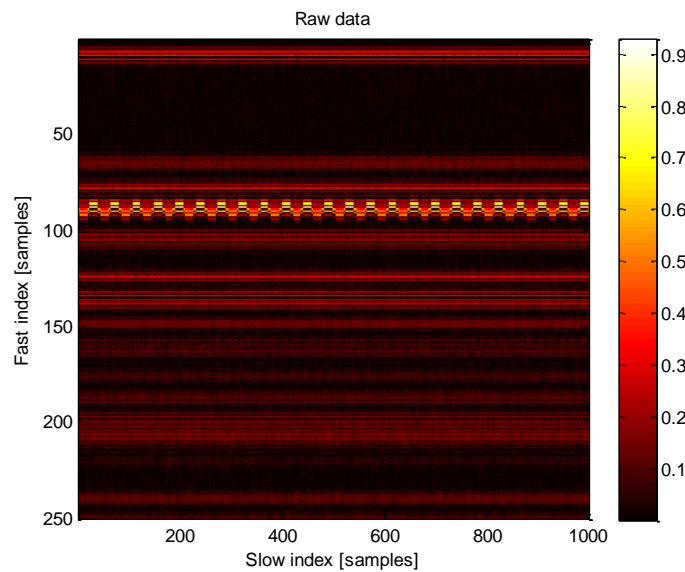


Fig 9: Heatmap of the received signal in the $\underline{\underline{Y}}$ matrix

In Figure 9 we see each captured waveform as a column, where the brighter the color, the higher the amplitude in that particular fast time index. So, this plot represents the progression of the channel response to our emitted pulses along the slow time axis.

In this plot we see some steady values along the slow index corresponding to the static channel responses presented in equation (3). Besides that, we see a sinusoidal multipath echo, which corresponds to the respiratory variations related to the chest patient, our signal of interest.

4.1.1.3. Clutter removal

Now, we start with the preprocessing of the signal to remove those steady scatters of the received signal before entering in the frequency analysis.

To accomplish that, we implement the equation (8) of our theoretical proposal with the simple built-in function *mean* of the Matlab software. The heat map result of that processing can be seen in Figure 10:

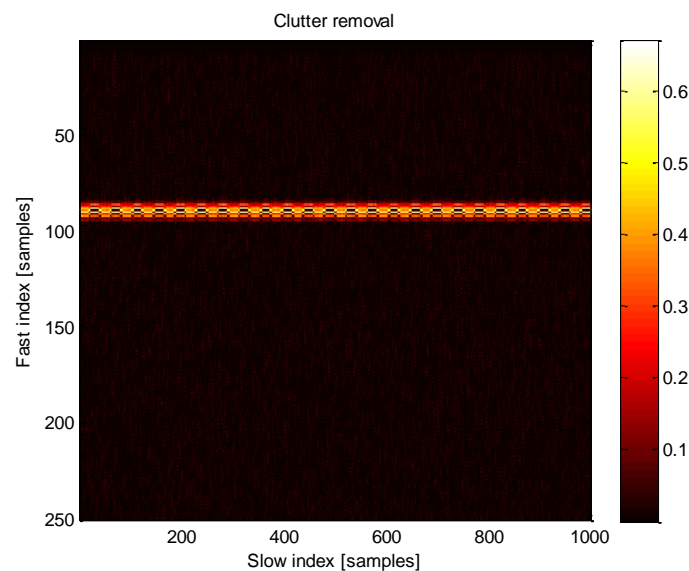


Fig 10: Heatmap of the received signal once the clutter is removed

In the Figure 10 above we see that any static contribution is successfully removed. We have to also highlight that the interest chest movement signal has been distorted by the residual term $x_0(m)$ in equation (8). But still, it maintains enough information to posterior processing of the signal.

4.1.2. Spectral techniques results

Before applying the FFT transform we need to estimate the optimal fast time index \hat{m}_0 to maximize the results of the frequency analysis, as discussed in Section 3.2.1 and detailed in (28).

Once we have that index, we apply compute the power spectral density using the Bartlett estimator in (9). The simulation parameters are depicted in Table 5.

Technique	Bartlett Estimation
-----------	---------------------

Target Frequency	0.24Hz
K	5
L	200
N_s	1000

Table 5: Bartlett estimation parameters

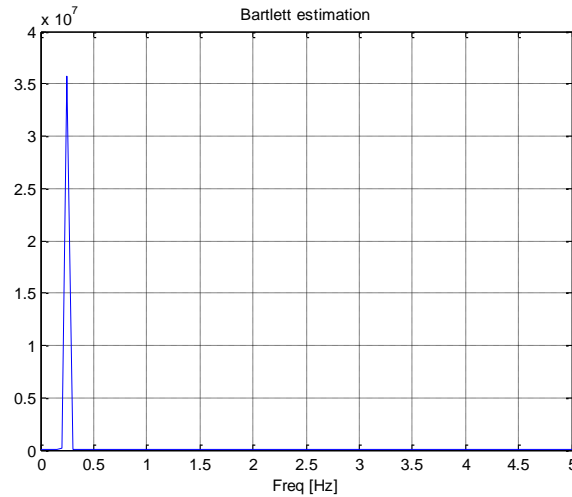


Fig 11: Bartlett estimation

Regarding the graphical results in Figure 11, we obtain the peak related to the chest frequency at 0.25Hz. This result differs a little with the real value (0.24Hz) due to the already explained characteristics of the Bartlett estimator. Apart of that, the peak is clear and without any distortion.

Continuing with the spectral techniques, we apply the mentioned method of averaged Bartlett estimations in equation (11). We use $M = 4$ to clearly see the contribution of each individual spectrum estimation:

Technique	Averaged Bartlett Estimation
Target Frequency	0.24Hz
K	5
L	200
M	4
N_s (for each Bartlett estimation)	1000

Table 6: Averaged Bartlett Estimation parameters

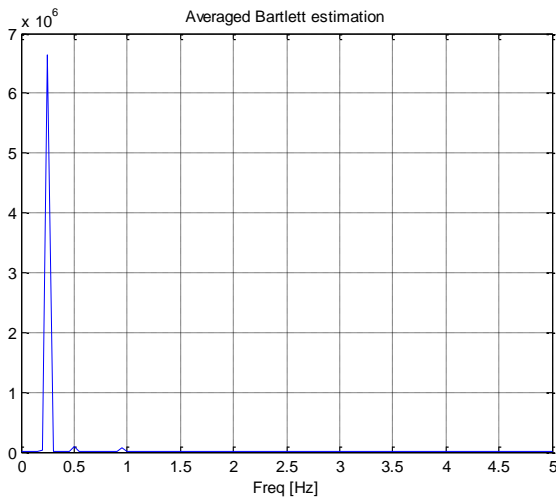


Fig 12: Averaged Bartlett estimation

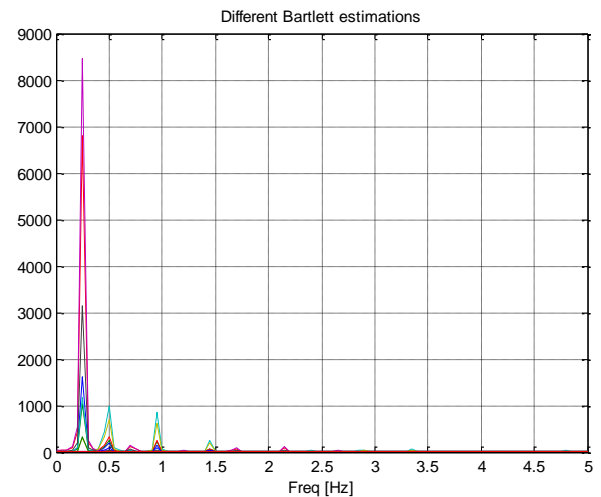


Fig 13: Different Bartlett estimations around the optimal index

With this method we see some little harmonic contributions due to non-optimal indexes and besides that, the same characteristics as in the Figure 11. In this simulated environment, the enhanced robustness of the method cannot be perceived. In later sections with real data we appreciate it better. Each single Bartlett contribution is represented in the Figure 13.

In these Bartlett estimations, we see different harmonic contributions in each case, relative to the different indexes. But, besides of that, we see that most of the signals contribute to the objective frequency with different amplitude levels. That is a fact that we are taking advantage of.

4.1.3. AR modelling

Now, through the AR modelling technique we see the spectral results over different coefficient calculations. We start with Block processing coefficients and then we follow with the LMS approach, as seen on the theoretical purpose.

As a first assumption, we work with only the most important fast time index found in equation (10), as the presented methods are only considered for one dimension.

4.1.3.1. Block processing coefficients results

As mentioned in the theoretical approach, one of the requirements of the AR modelling is the selection of some parameters (as number of coefficients p in this case) to adjust our model to the real signal in exchange of better frequency resolution.

To select the proper number of coefficients, arbitrarily we choose 8 as start value, as we were obtaining enough precision for our application. Due to the nature of our signal, if we chose a number of filters lower or equal than 7 we are not be able to properly detect the desired peak. And if we start increasing the number of filters, the response of the system is more fitted to the real spectrum of the signal. As consequence of that, unnecessary harmonics shows up, which can be even produce misleading results in the peak detection. Also the computational workload unnecessary increases.

In this first approach, we use Matlab functions as *xcorr*, together with the *toeplitz* method to build the correlation matrix needed in equation (18). Once we have obtained the coefficients, we plot the spectral density estimation from the AR model coefficients using equation (11):

Technique	AR Power Spectral Density Estimation
Target Frequency	0.24Hz
<i>p</i>	8
<i>N_s</i>	1000

Table 7: AR Power Spectral Density Estimation parameters

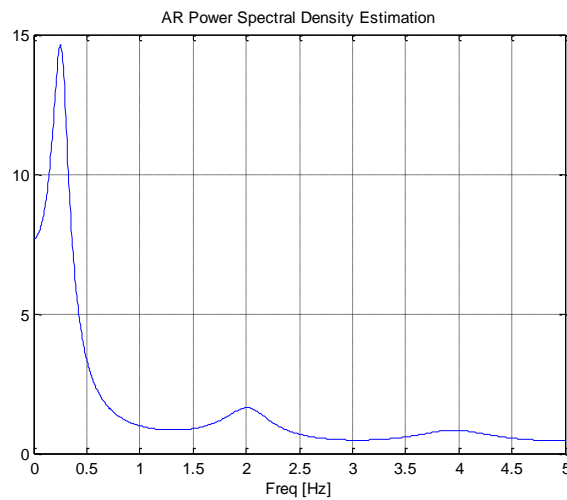


fig 14: AR power spectral density estimation

As we can see in the previous Figure 14, the spectral density estimation is smothered in comparison with the Bartlett approach in Figure 11 and 12. Also we could highlight that at first sight the results are more precise, as we are getting closer results to the 0.24Hz. Although we cannot state that this method has better precision only with one realization, this higher precision was expected from the already presented theoretical study.

4.1.3.2. Adaptive coefficients results

As mentioned, in the AR modelling we have to choose some parameters to get a well suited modelling of our real signal. In the case of the LMS approach, we have some additional parameters to tune up, and with it, obtain different system responses.

Those parameters are the number of coefficients *p* (as in the previous case), the update step μ and the coefficient initializations.

4.1.3.2.1. Zeroes initialization

About the configuration of the system, first we start with a vector of zeros as initialization of the coefficients, an arbitrary step of $\mu = 1$ (accomplishing the restriction in equation (30) with $\lambda_{max} = 1$, given that the signal is normalized) and $p = 12$ coefficients. Later, we comment the combination of those two last parameters and how they affect the system response:

Technique	LMS
Target Frequency	0.24Hz
p	12
μ	1
Initialization	Vector of zeros
N_s	1000

Table 8: LMS with zeroes initialization parameters

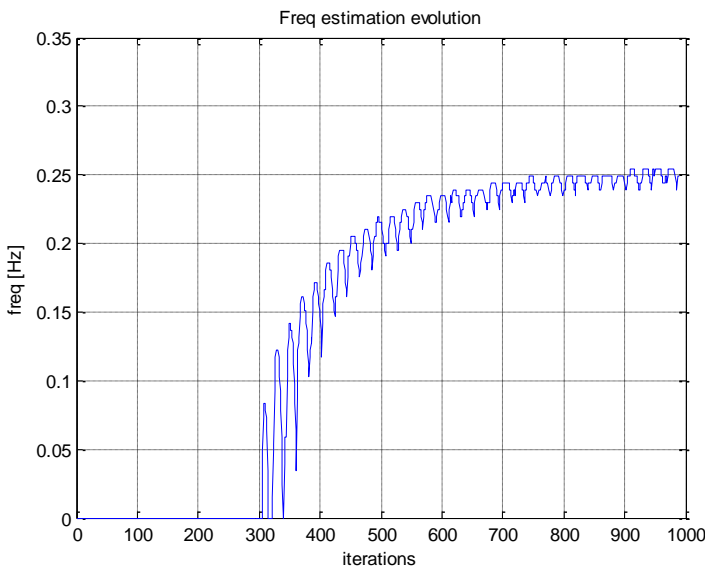


Fig 15: Frequency estimation evolution over the iterations of the algorithm (zeroes initialization)

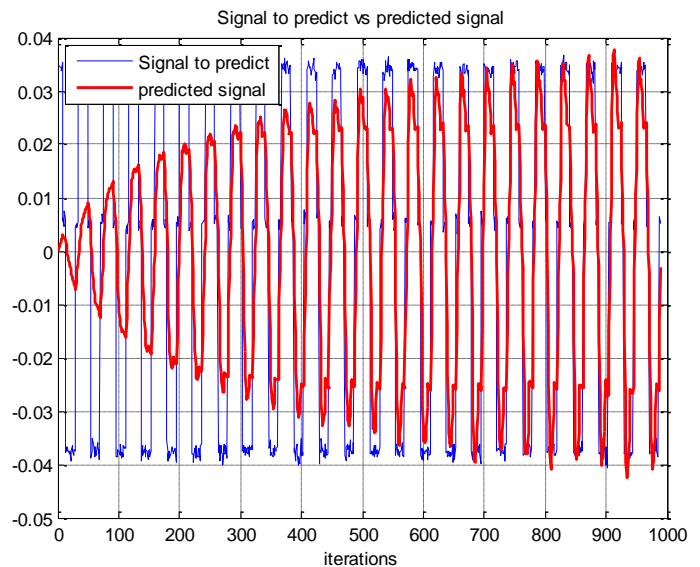


Fig 16: Predicted signal, in front of signal to predict over the iterations of the algorithm (zeroes initialization)

As we can see in Figure 15, the system properly detects the breath frequency converging in the range of $0.244\text{Hz} - 0.249\text{Hz}$.

At first sight, we could think that as soon as the predicted signal is adapted to the signal to predict (Figure 16) the frequency prediction should already reach the right estimated value. The reality is that as aforementioned in section 3.2.2, the AR Spectral estimation is sensible to errors in the coefficient values. So, we have to wait for the signal to really finish its adaptation and fit the signal to predict as tightly as possible to have proper spectral density estimations.

Thus, those values at 0Hz are related to the peak detection in those particular estimated spectral density representations at the first stages of the algorithm. In those first estimated spectral density representations the peak related to the estimated frequency is not the highest one yet given the early evolution of the coefficients.

In Figure 16 and corresponding with the estimated frequency, we can see the progressive adaptation of the predicted signal (red) in front of the signal to predict (blue). We can see a really good adaptation in the last periods given the regularity and steadiness of the oscillation of the simulated signal.

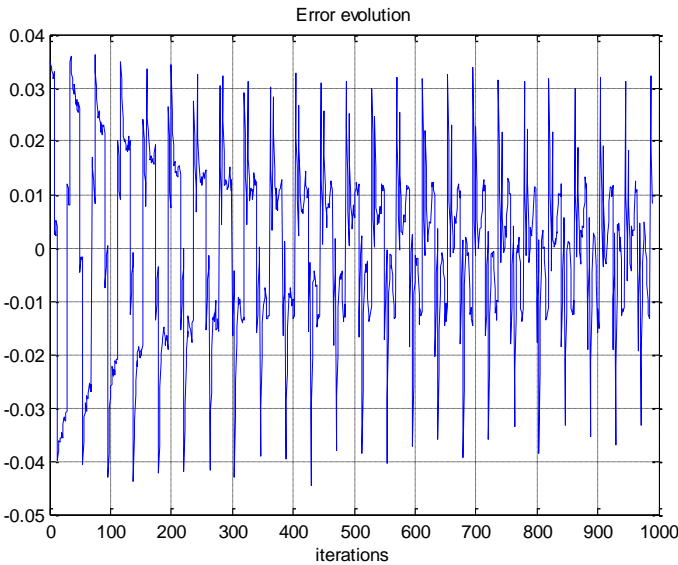


Fig 17: Prediction error evolution over the iterations of the algorithm (zeroes initialization)

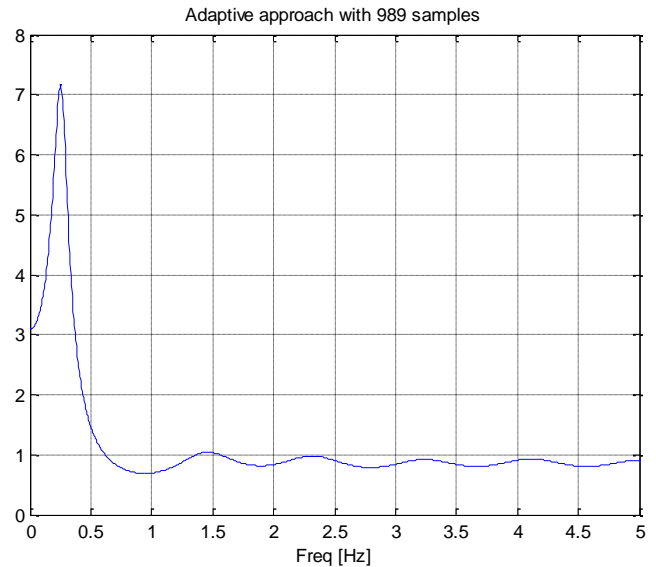


Fig 18: Final spectral density estimation with LMS approach (zeroes initialization)

Now, we analyze the representation error evolution of equation (20) in Figure 17. At the very first periods we are visualizing the error with the same shape as signal to predict, given that the signal prediction starts at null value and consequently we are not yet able to compensate it. As we move forward in the plot, the progression ends up in a shape which is pretty close to white noise, which corresponds to the added noise contribution that the predictor cannot foretell.

And Figure 18 is the representation of the spectral density of the last iteration of equation (11). The plot is quite similar to the results of the block processing calculation Figure 14 in previous stages.

4.1.3.2.2. Block coefficients initialization

With the same exact settings as before, but initializing the system with the precalculated filter coefficients obtained with a block processing of N_0 samples (with $N_0 \ll N_s$). In this case, for $N_0 = 15$:

Technique	LMS
Target Frequency	0.24Hz
p	12

μ	1
Initialization	Block of N_0 coefficients
N_0	15
N_s	1000

Table 9: LMS with block initialization parameters

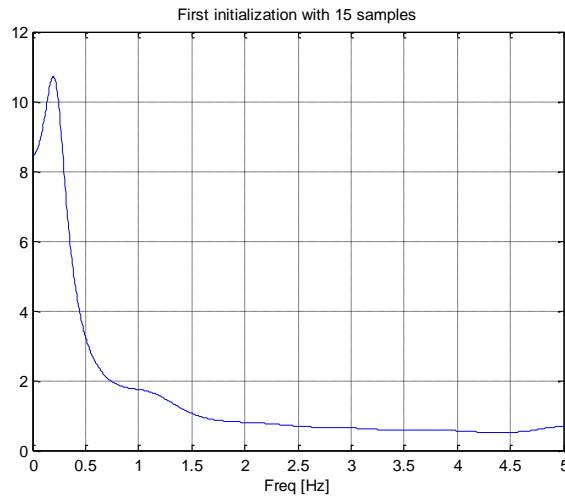


fig 19: Spectral density estimation of the initialization block with 15 samples

First, this is the spectral density estimation of the initialization with only 15 samples. As we can see in the peak, we are getting good first approximation (0.19Hz) given the low number of required samples.

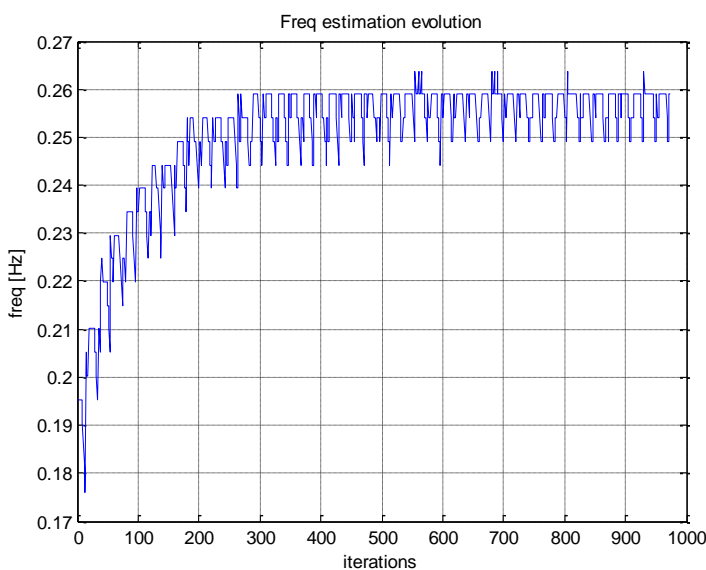


Fig 20: Frequency estimation evolution over the iterations of the algorithm (block initialization)

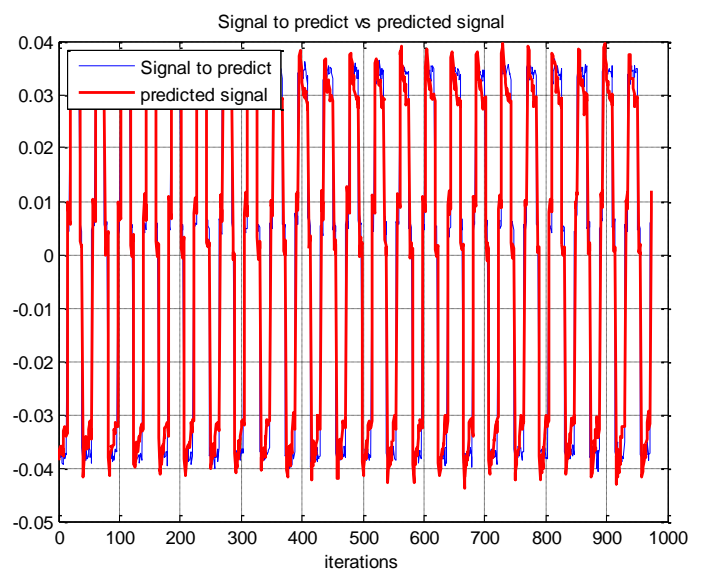


Fig 21: Predicted signal, in front of signal to predict over the iterations of the algorithm (block initialization)

If we compare this frequency evolution graph in Figure 20 with the one with zeros as initialization in Figure 15 we can realize some interesting differences. First, the steady error margin is the same, although it seems bigger in this last one. That is because of the Matlab representation, which has a larger dynamic range in the zeroes initialization. The steady error is the same because it is related with the update step, which is equal in both cases. Second, the system in Figure 20 reaches the steady oscillation much faster. In the previous case of Figure 15 we were reaching it at the 650th iteration, while in this case we already have it at the 200th iteration. And third, the converged frequency estimation value in this case has a little shift in mean of approximately 0.01 Hz. To solve that, and taking into account that with this initialization we reach faster the steady error state, we could lower the update step.

In the signal prediction plot in Figure 21 we see the expected response. Already in the first periods the prediction is really good and as we move ahead on the progression the prediction gets more fitted.

4.1.3.2.3. Frequency shift response

Now that we have checked the response of the system to different initializations, we are going to proceed with testing the adaptation of the system in front of a frequency shift in the signal, which is a required functionality to be able to detect respiratory variations like apnoea episodes or sudden increases in the respiratory rate (due to a tachycardia episode, for example).

To do so, we modify the generation of the breath signal loop adding a new statement. At half of the signal length we are going to double the breath frequency. Maintaining the same exact setup as in the last case the results are the following:

Technique	LMS
Target Frequency	0.24Hz (1 st section) & 0.48Hz (2 nd section)
p	12
μ	1
Initialization	Block of N_0 coefficients
N_0	15
N_s	1000

Table 10: LMS with frequency shifted signal parameters

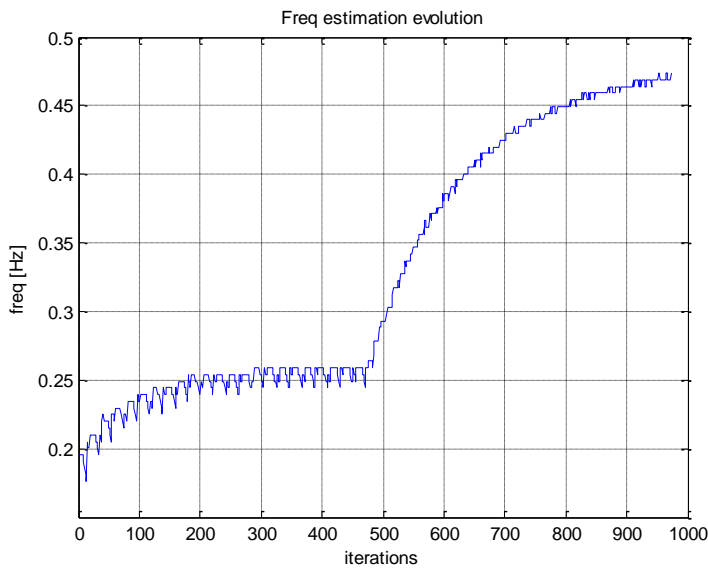


Fig 22: Frequency shifted signal. Frequency estimation evolution over the iterations of the algorithm (block initialization)

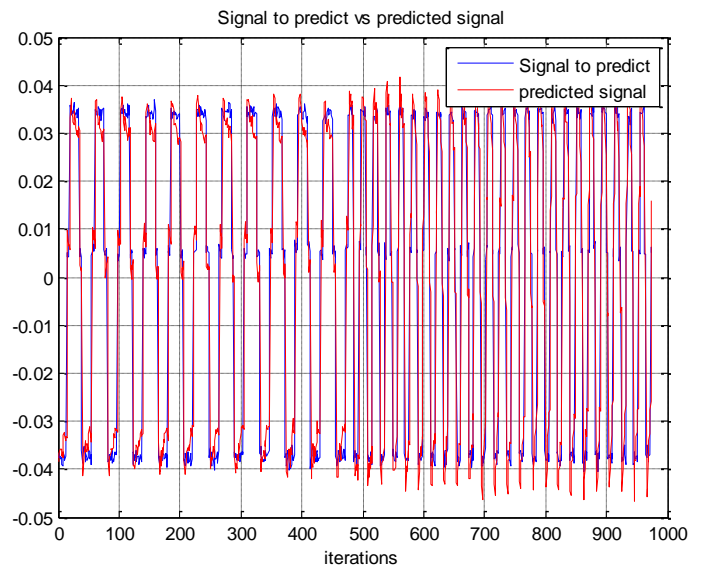


Fig 23: Frequency shifted signal. Predicted signal, in front of signal to predict over the iterations of the algorithm (block initialization)

In the frequency evolution plot, Figure 22, we can see the frequency shift and the corresponding pair of converges. First around 0.25Hz (we still have the little shift) and finally 0.47Hz, which is really close to $0.24 \times 2 = 0.48\text{Hz}$. If we compare both halves of the plot, in the first case we are getting to the right value fast enough, but in the second half we need the whole trace to arrive finally at the desired value.

In the signal prediction, figure 23, we see proper results. At first sight the adaptation is proper, and even in the frequency shift the system doesn't lose a single period. May this good adaptation in the shift be due to that we are doubling the frequency, and seems that for the system it is easier to readapt to a multiple of the original frequency. To fix that slow adaptation we tweak the coefficient numbers and update step in the next sections:

Technique	LMS
Target Frequency	0.24Hz (1 st section) & 0.48Hz (2 nd section)
p	22
μ	1
Initialization	Block of N_0 coefficients
N_0	15
N_s	1000

Table 11: LMS with frequency shifted signal and increased coefficients parameters

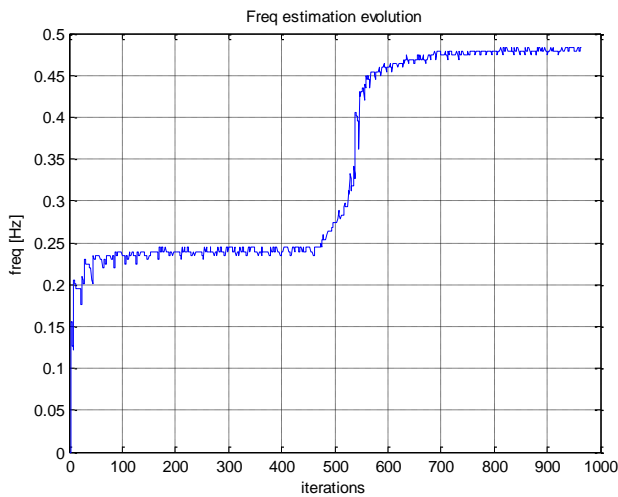


Fig 24: Frequency shifted signal. Frequency estimation evolution over the iterations of the algorithm (block initialization and increased coefficients, table 11)

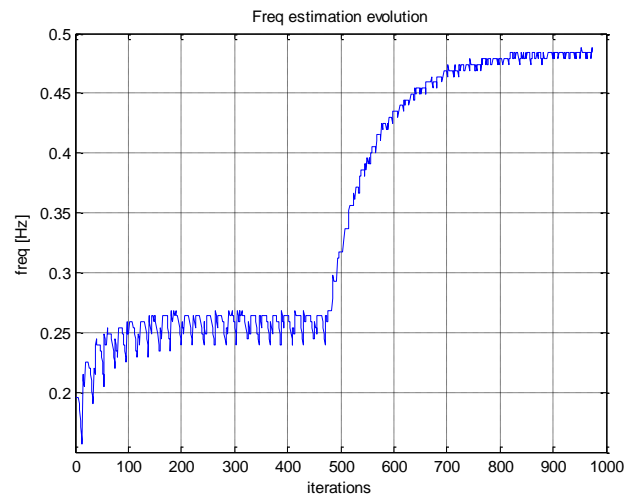


Fig 25: Frequency shifted signal. Frequency estimation evolution over the iterations of the algorithm (block initialization and increased update step, table 12)

In this Figure 24 we have increased the number of coefficients from 12 to 22. If we analyze the plot we see an enhanced response in many aspects. To begin with, we get closer to the 0.24Hz in the first stage (0.2394Hz). And regarding the second stage, we get faster to the steady oscillation with 0.478Hz.

Logically, and given those results, we can state that the more coefficients that we have in our system, the better the general response is, in both terms of converging speed and steady error.

In the other hand, if instead of increasing the number of coefficients we increase the update step from $\mu = 1$ to $\mu = 2$ we get to:

Technique	LMS
Target Frequency	0.24Hz (1 st section) & 0.48Hz (2 nd section)
p	12
μ	2
Initialization	Block of N_0 coefficients
N_0	15
N_s	1000

Table 12: LMS with frequency shifted signal and increased update step parameters

In this plot in Figure 25 we get similar results to the one with increased coefficients in Figure 24, but with worst characteristics in some sections. First, we are still converging at ~ 0.25 Hz given the lesser precision. And second, we arrive later to the optimal value in the transition.

But still, the response is considerably better in some aspects with no extra computational cost. As already mentioned, we should find a compromise between all those settings to adapt our system to the real world operating regime.

4.1.4. Monte-Carlo simulations

At this point, once we have illustrated with particularly significant cases the behavior of each of the estimation solutions, we present a set of simulations to study the general response of such solutions.

To better understand the characteristics of the solutions we represent its responses associated to different noise levels. To obtain results for a particular noise level, we generate a number of different UWB channel realizations from the chosen model, and for each of them, we generate a corresponding simulation of a patient breathing as described in Section 4.1.1.2. with the according noise level. Then, we apply the solution under consideration to all of those generated simulations. Applying the solution to the generated set of simulations which are based in different channel realizations allows us the extraction of averaged results of the parameters to estimate, and with it, obtain results which are less depending in a particular channel realization. We then sweep across all the noise levels in a defined range replicating the just mentioned method to obtain the progression of characteristics to analyze. The characteristics of the solutions that we illustrate are the averaged frequency estimation and the RMSE (Root Mean Square Error) of the estimation.

The RMSE plot gives us a notion of distance (in Hz) between the estimated respiratory rate and the target frequency. This figure provides us more insights of the error progression, since it has the same units as the quantity plotted on the vertical axis in front of, for example, the straight MSE which its units are the squared value (Hz^2 in this case).

We present a series of graphs where we observe the progression both the mentioned characteristics in front of the noise level.

Number of channels	300
Target Frequency	0.24Hz
SNR range	-30 to -5dB
N_s	1000

Table 13: Monte-Carlo simulations parameters

We analyse each of the solutions following the Monte-Carlo parameters defined in Table 13. Within each particular case, we specify the configuration of the estimator and then we illustrate and present the statistical results.

4.1.4.1. Averaged Bartlett estimator

In this first situation we evaluate the characteristics of the mentioned Averaged Bartlett estimator. The configuration of the estimator is the same as the one used in the illustrative case of Section 4.1.2, specified in table 6.

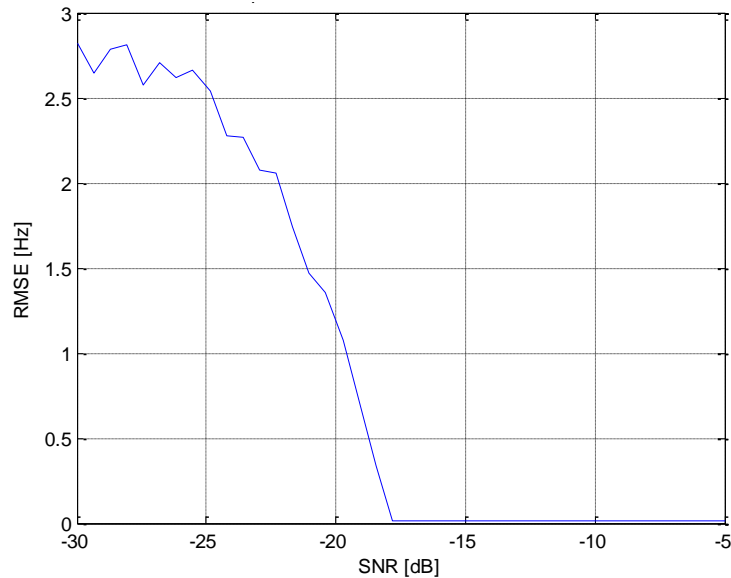


Fig 26: Root Mean Squared Error of the estimation, Bartlett Estimator

Starting by Figure 29, in the trace related to the Bartlett Estimator, first we visualize some oscillation around 2.5Hz at the lowest values of SNR, continuing to a steep descend towards the final estimated value (0.25Hz) starting from -25dB and reaching it at around -16dB . The detected averaged frequency of 2.5Hz in the first and lowest values of the SNR is due to the total random results obtained because of the effect of the noise masking the respiratory rate signal. Specifically, we obtain 2.5Hz , which corresponds the mean value between 0 and 5Hz , the maximum and minimum possible ranges to measure. Following the same progression and accordingly, the RMSE representation of Figure 26 depicts a clear decay towards the minimum error following the transition from totally noisy measurements to meaningful measurements.

4.1.4.2. AR block processing coefficients

Following the analysis, we evaluate the results of the AR spectral density estimation with the obtention of the coefficients in block. The configuration of the estimator is the same as the one used in the illustrative case of Section 4.1.3.1, specified in table 7.

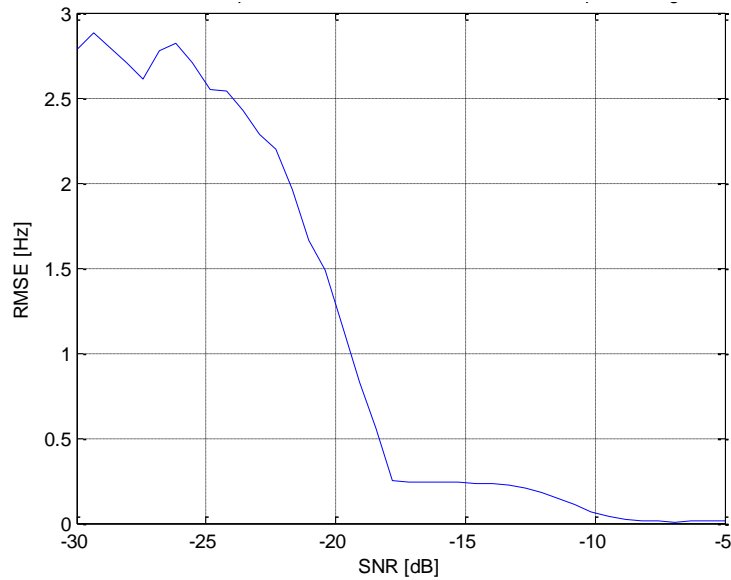


Fig 27: Root Mean Squared Error of the estimation, AR block processing

The progression in the trace related to the AR block processing in Figure 29 is similar at the beginning to the one of the Averaged Bartlett estimation due again to the excess of noise, but differs at getting stuck at 0Hz in the range from $-17dBs$ to $-10dBs$, where we finally detect the right respiratory rate. In the RMSE we can see both decays, first, the one related to entering in a zone not masked by noise, and the second one, with a much smoother slope corresponding to the section where we successfully detect the respiratory rate value.

4.1.4.3. AR Adaptive coefficients

The used configuration of the estimator is specified in table 8 and based in the case of Section 4.1.3.2.2, but increasing the number of coefficients to 20 (closer to the real experiment setup, where we need a higher number of coefficients to obtain proper results).

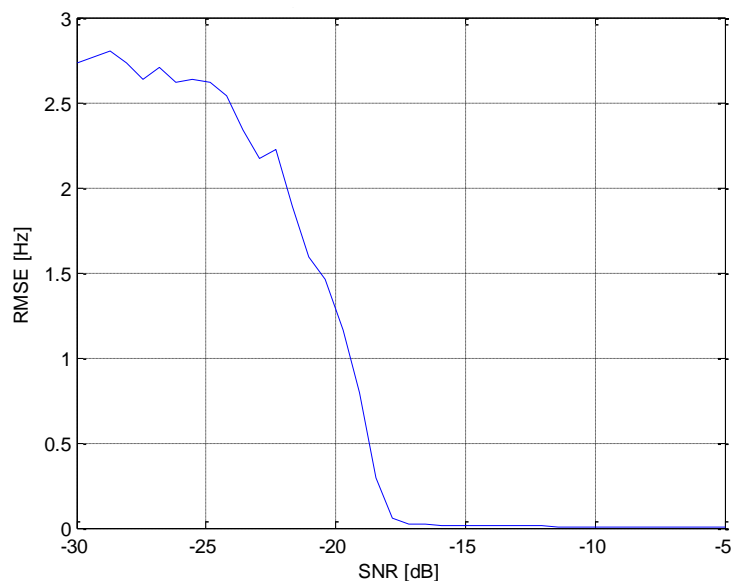


Fig 28: Root Mean Squared Error of the estimation, AR LMS

Finally, in the adaptive coefficients approach (LMS estimator) in Figure 29, the estimated frequency decays in the first stage with the same shape and position as in the past systems. But, in difference with the other two estimators, once it gets to a relatively good result at -17dBs it keeps improving its accuracy on the estimation, as seen in the close-up of Figure 30, heading to the lowest RMSE of the three systems at the end of the graph.

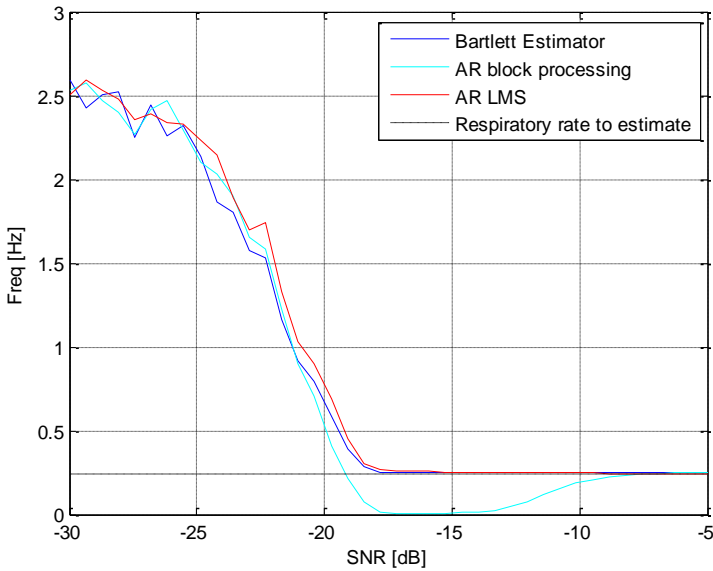


Fig 29: Averaged Estimated Frequency of all three estimators

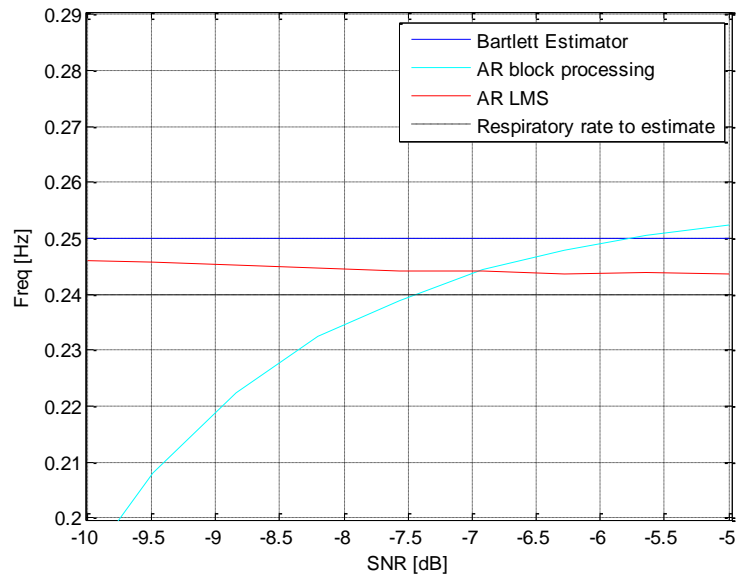


Fig 30: Averaged Estimated Frequency of all three estimators (close-up of the last 5 dBs)

If we want to do a general evaluation of all three estimators, we have to highlight the difficulty of proposing a fair comparison between them, given that each solution depends on different parameters (signal length, coefficients, update step, etc.). Considering that, it is clear that the large number of samples generated for each simulation ($N_s = 1000$) works in favour of the Spectral techniques results, outperforming the AR with block processing and getting a similar shape to AR LMS trace. In an experimental setup with less available samples, the AR modelling approach would take advantage of its parametric configuration, yielding better results in more hostile scenarios. At its part, the LMS estimator, in addition of being the only approach able to work in real-time, shows good performance as aforementioned. This can also be a consequence of the large number of samples, given that depending of the update step of the LMS algorithm (in this case it is not set at the theoretical maximum), it takes a higher number of iterations to achieve the most precise results.

4.2. Experimental results

In this last section we are going to test our algorithms into real data extracted from experimental realizations. At the same time we validate our initial suppositions in the modelling and see the real response of our system.

4.2.1. Equipment description

First of all, we further introduce the used equipment to perform such measurements.

The used device is PulsON 410 Series, this hardware device by Time Domain is a small and low power coherent UWB module. Depending on the software used in the hardware

module we can obtain different operation modes. For example, if we use the RCM (Ranging Communications Module) our hardware works as a ranging and communication terminal. On the other hand, if we use the MRM (Monostatic Radar Module) or CAT (Channel Analysis Tool) we obtain radar capabilities. In our case we use the MRM module to use the hardware as a standalone monostatic radar.



Fig 31: PulsON 410 MRM with both antennas connected

The main characteristics of our device are:

- Good performance in high multipath and high clutter environments
- Coherent signal processing extends operating range at low signal power levels
- P410 MRM provides raw scans for post processing
- UWB chipset enables low cost, small size, and low power operation
- UWB waveform and pseudo random encoding ensures noise-like transmissions with a very small RF footprint
- Seven separate channels provided
- RF transmissions from 3.1GHz to 5.3GHz, with center at 4.3GHz
- Two user-configurable antenna ports for dual antenna operation
- RF emissions compliant with FCC limits
- Single 7.6 x 8.0 x 1.6 cm board
- USB or Serial interface
- Several sleep modes allow user to reduce power consumption

Another high important characteristic of the hardware is that it has a C and, more importantly, Matlab API, which suites for our prototyping development.

4.2.2. Experiment setup

Most of the test measurements are performed in the Engineering Lab of the CTTC. Actually, we could consider that environment as a pretty hostile scenario. The laboratory is composed by several metal scatters (metal structures, computers, shelves, etc.) so the static interferences are going to be of a great importance.

Besides the Lab environment, we first start doing measurements in the anechoic chamber of the CTTC. There we expect to obtain clearer measures given the fact that we obtain much less reflections and scatters.

To perform the measurements in both environments we follow a simple structure:

- We connect the HW device to the computer through the USB cable and we place it on the edge of the lab table (or metal structure in the anechoic chamber)
- We place the sitting subject approximately at 1.5 m (3 m in the anechoic chamber) of the device with clear LOS

- We aim the device and its antennas (even though they are omnidirectional) to the chest of the subject
- We perform the measures

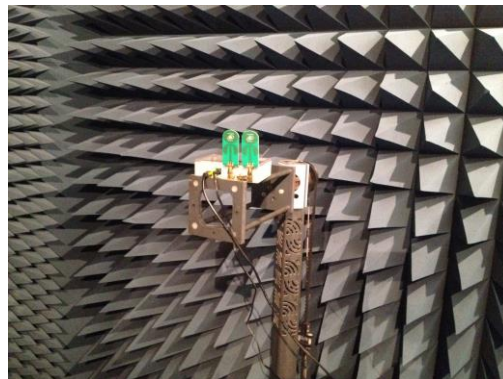


Fig 32: Device setup in anechoic chamber

The needed time to obtain a set of samples to work with in an offline regime is about 50 seconds to get 500 samples (sampling at 10Hz).

In the schematic representation of Figure 33, we can see the interaction between our host computer and the P410 module through the API calls and responses. At the same time, the P410 is in charge of performing the UWB sensing towards the patient represented at the rightmost. In our use case, the P410 module is configured to return raw scan data, without any of the additional processing (like motion filters) implemented by default in the HW device. We deal directly with the raw data to gain complete control of the signal processing.

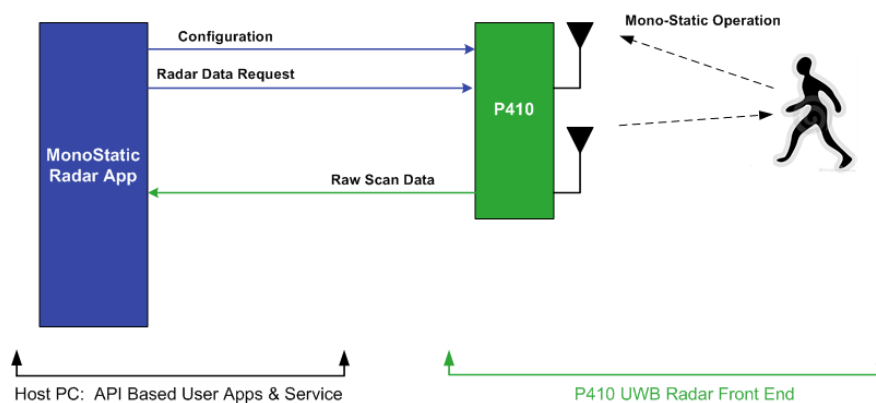


Fig 33: Scheme of the measurement set up

4.2.3. Anechoic chamber results

The results that we are going to present are from a subject whose breath frequency was of 0.24Hz . The slow time sampling frequency we set to 6Hz . To measure this real value in the anechoic chamber and in the lab results we have used the methodology most commonly used in real cases at hospitals: count the number of breathings and measuring the total lapsed time.

First, we start by visualizing the data in the heatmap plots:

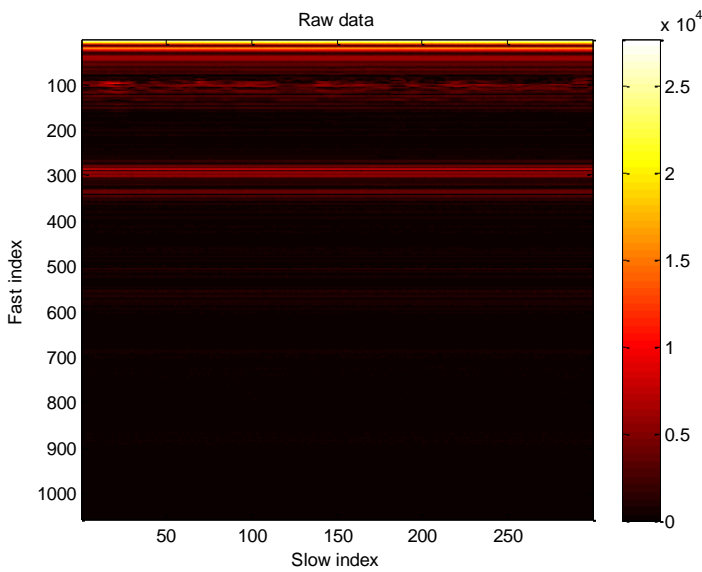


Fig 34: Raw data heatmap, anechoic chamber

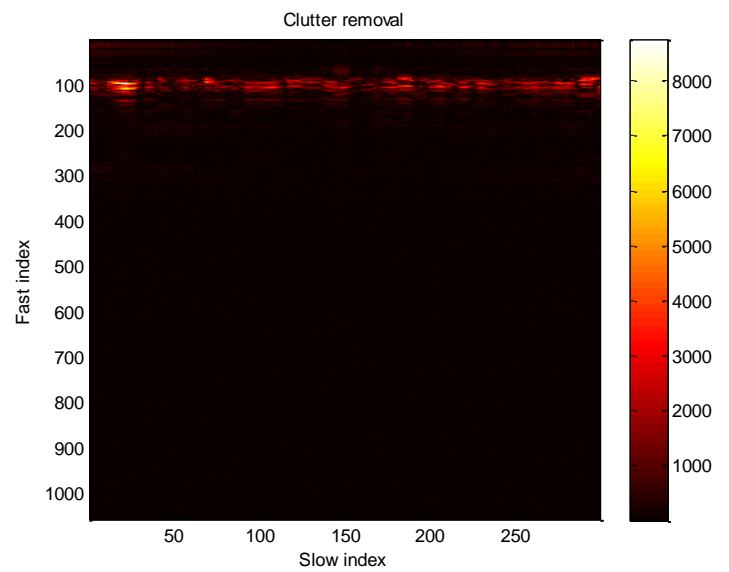


Fig 35: Clutter removal heatmap, anechoic chamber

In both plots we obtain the coherent results with the simulations. Starting from the raw data heatmap in the Figure 34, we visualize the variation of the chest movement around the 100th fast sample index. Also, besides that, we see some other dimmed static scatters. Those can be due the external structure to hold on the computer inside the chamber or also due to the non-completely closed door of the chamber.

If we continue with the clutter removed one at Figure 35 we can see that the steady scatters are removed completely and we only see information related to the chest movement.

In general, we can highlight some insights from the first approach to the real data. First, both plots in Figure 34 and 35 look similar to the ones generated in the simulations, so we could assume that the model chosen was right and coherent with the reality. And second, the chest movement cannot be seen clearly at first sight as in the raw heatmap of the simulations, instead of that, we can see a slight modulation over the first fast time samples of the matrix.

4.2.3.1. Spectral techniques results

If we apply the first spectral technique, the averaged Bartlett estimation we obtain:

Technique	Averaged Bartlett estimation
Target Frequency	0.24Hz
K	2
L	150
M	4
N_s	300

Table 14: Averaged Bartlett estimation parameters, anechoic chamber

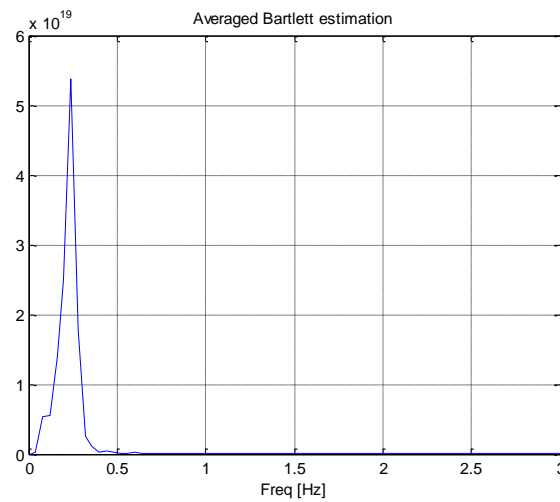


Fig 36: Averaged Bartlett estimation, anechoic chamber

In the Averaged Bartlett estimator we see a clear peak, with almost no harmonic contribution. Also, the result 0.238Hz considerably close to the 0.24Hz to estimate. This first frequency result is still coherent with the simulated model, as we are already seeing from the first plots in Figures 34 and 35.

4.2.3.2. AR modelling results

In this case, for the same number of coefficients as in the simulations $p = 8$ we apply our AR modelling solution, which leads to:

Technique	AR Power Spectral Density Estimation
Target Frequency	0.24Hz
p	8
N_s	300

Table 15: AR Power Spectral Density estimation parameters, anechoic chamber

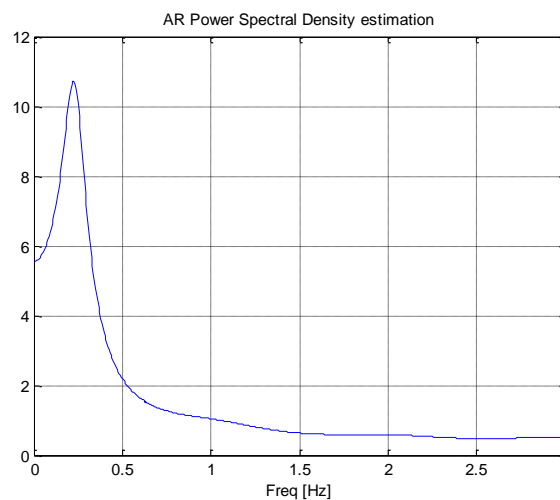


Fig 37: AR Power Spectral Density estimation, anechoic chamber

The obtained result, 0.2238Hz is a little distant from the original value, but still we detected the right peak. This result could be due to some low frequency contributions that our motion filter could not discriminate. Those movements were related to the steadiness of the measured patient, which in this case was standing instead of sitting (as in the laboratory measurements).

4.2.4. Laboratory results

In this case, the subject's breath frequency was of 0.25Hz and he was positioned according to the Experiment setup section. The sampling frequency of these tests is now the proposed in the theoretical study, 10Hz .

We start by representing the heatmap matrix of the measured signals. First, directly from the device and then, the clutter removal one:

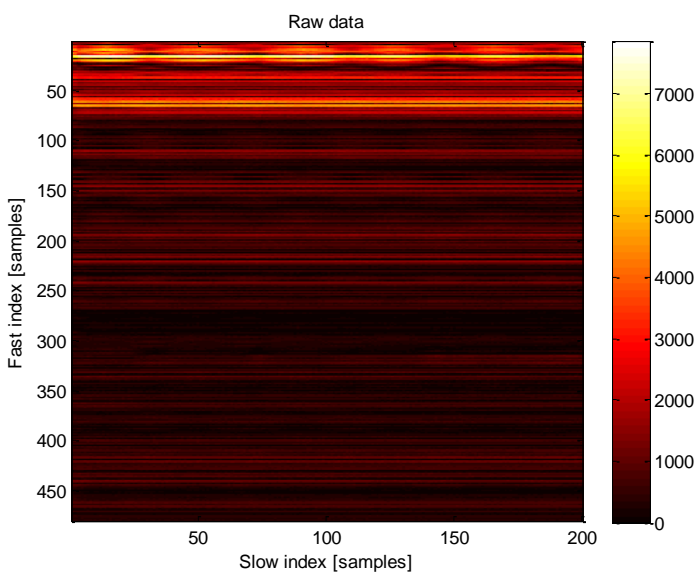


Fig 38: Raw data heatmap, laboratory

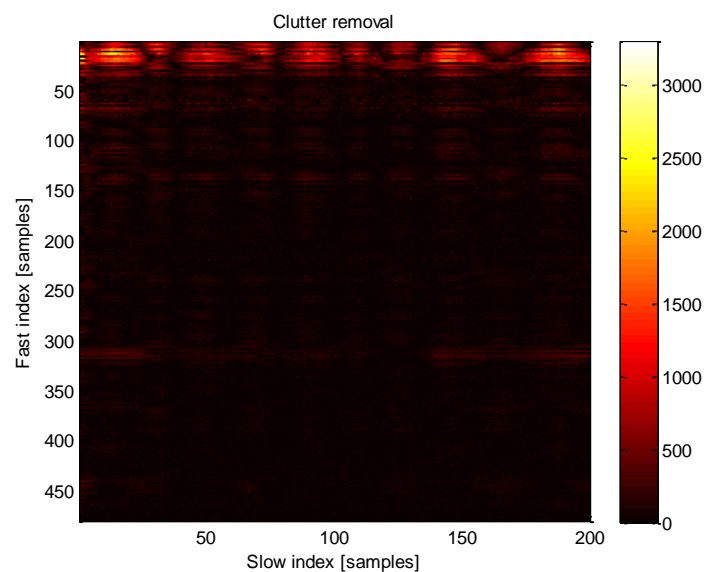


Fig 39: Clutter removal signal, laboratory

In this plot in Figure 38 we can observe a lot more static contributions in comparison with Figure 34 in the anechoic chamber. Besides that, the measuring was quite stable, allowing us to almost visualize the oscillation of the chest movement at first glance in the first samples of the fast time index.

Seeing the clutter removed heatmap in comparison with the anechoic chamber results in Figure 35, we have more residual signals corresponding to secondary reflections along the fast time index. But still, and coherently with the first plot, we can spot the moving reflections with enough clarity.

We see the frequency results in the following sections, and with it, if our system is capable to handle real experiment data in a hostile scenario:

4.2.4.1. Spectral techniques results

Applying the first method of Averaged Bartlett estimation we obtain:

Technique	Averaged Bartlett estimation
-----------	------------------------------

Target Frequency	0.25Hz
K	2
L	200
M	4
N_s	400

Table 16: Averaged Bartlett estimation parameters, laboratory

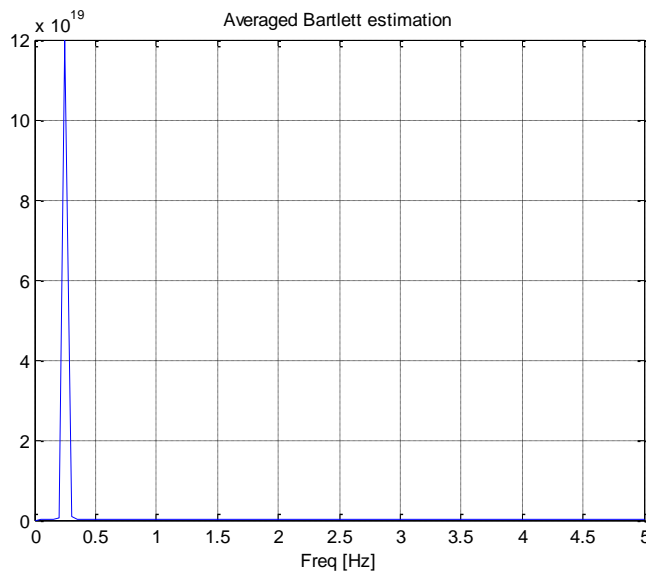


Fig 40: Averaged Bartlett estimation, laboratory

Leading to good results with predicted frequency at 0.25Hz. The shape of the obtained spectrum is really close to the obtained in the simulations. Once more, the results of now a completely non ideal scenario (with high static scatter contribution) leads to predicted results in the simulations and theoretical approaches.

4.2.4.2. AR modelling results

Given the good results on the spectral techniques analysis, we apply the AR modelling solutions.

4.2.4.3. Block processing coefficient calculation

In our first proposal for AR modeling with block processing calculation we obtain:

Technique	AR Power Spectral Density Estimation
Target Frequency	0.25Hz
p	10

N_s	400
-------	-----

Table 17: AR power spectral density estimation parameters, laboratory

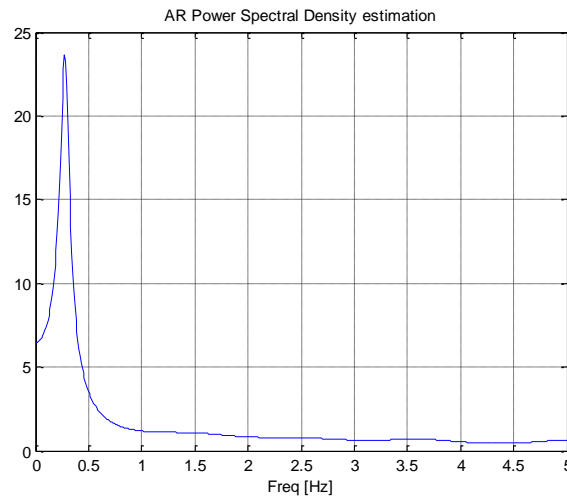


Fig 41: AR power spectral density estimation, laboratory

In the above plot we can see a good approximation to the right value, getting the 0.2508Hz. In the simulation scenario we implemented our LP solution with 8 coefficients, being this number the minimal number of coefficients that was giving us good enough estimations. But, in this real data case 8 coefficients weren't enough given the inherent irregularities in the signal. We were getting the right peak but it was slightly shifted in frequency. To ensure good results we gave some margin by selecting 10 coefficients.

4.2.4.4. Adaptive coefficients results

As we have already done with the other estimators, now we are going to apply the LMS based solution to real data. First, we start with the same measurement to have the same reference, also, we are going to use the same LMS setup as in the simulations. We set $p = 20$, update step $\mu = 1$ and zeroes initialization. We chose that initialization given the first instabilities in the measuring. The results are the following:

Technique	LMS
Target Frequency	0.25Hz
p	20
μ	1
Initialization	Vector of zeros
N_s	200

Table 18: LMS parameters, laboratory

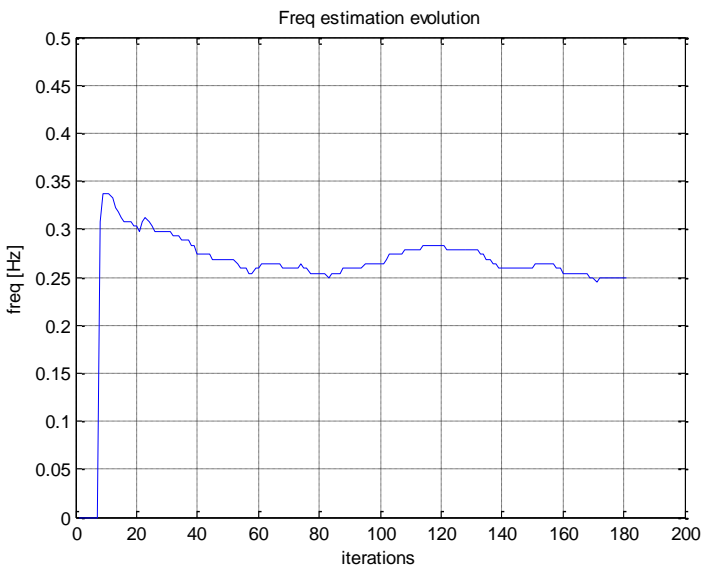


Fig 42: Frequency estimation evolution of LMS algorithm, laboratory

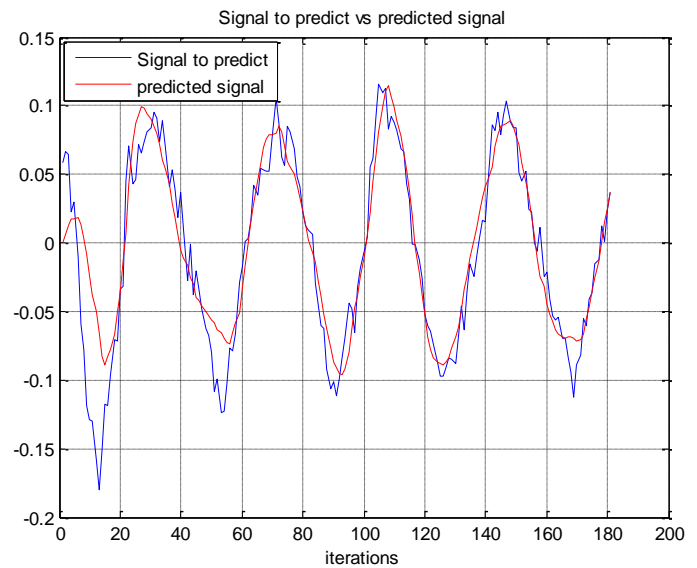


Fig 43: Signal to predict in comparison with predicted signal, laboratory

In Figure 42 we can see that with this implementation we estimate values oscillating really close from the original, ending at 0.25Hz. If we further analyze it, we can see that the filter detects the right frequency component really fast thanks to the increased number of coefficients. Also we could highlight that given the instability of the signal the system maintains the estimated value most of the time, only staying away from the original value at the beginning, while the system is stabilizing.

In Figure 43, in the prediction of the signal we can see a rapid adaptation increasing the amplitude gradually, until we reach the adaptation. Ending in the system adjustment quickly.

4.2.4.5. Frequency shifted measurements (apnoea episodes)

At this point, we need to test the system over a kind of frequency shifted measuring to check the algorithm response.

To start with, we use a new measuring. We concatenate first, a steady respiratory rate at 0.3Hz, continuing with a section of signal without chest movement (apnea episode) and finally we come back breathing at a higher frequency, 0.5Hz. We have combined this different respiratory rates in the spite of simulate a real apnea episode, in which the returning respiration rate in which the patient breathes again may be different (normally higher due the lack of oxygen).

If we now apply the LMS approach with the following configuration we obtain:

Technique	LMS
Target Frequency	0.3 Hz (from 0 - 150) 0 Hz (from 150 - 300) 0.5 Hz (from 300 - 500)

p	45
μ	2
Initialization	Vector of zeros
N_s	500

Table 19: LMS algorithm setup for respiratory patterns (apnoea) detection parameters, laboratory

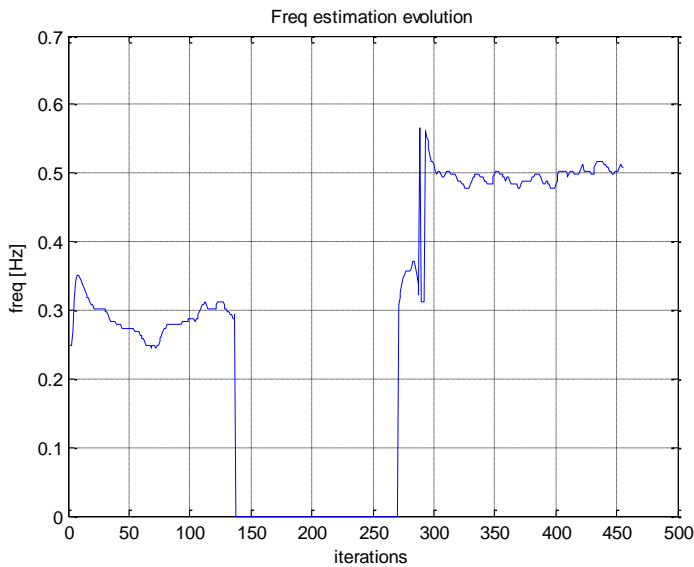


Fig 44: Frequency estimation evolution of LMS algorithm, laboratory

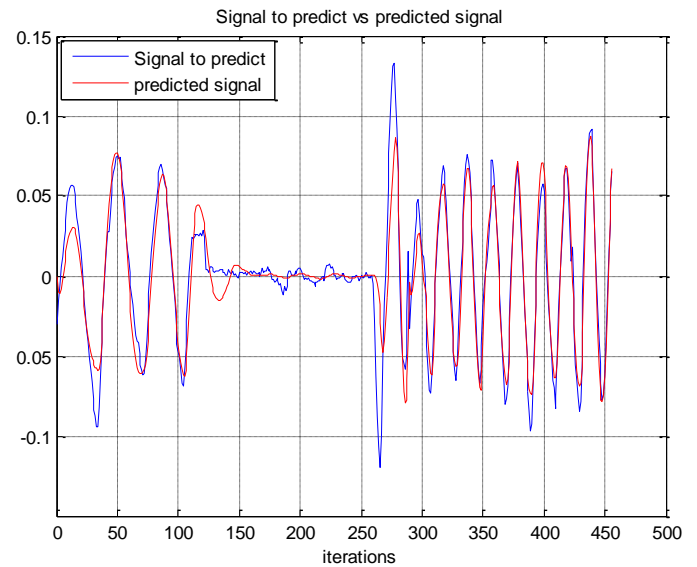


Fig 45: Signal to predict in comparison with predicted signal, laboratory

As it is depicted in Figure 44, the system successfully detects the frequency variation and falls towards 0Hz quickly. In fact, the first measurement at 0Hz is around the 138th sample. If we take into account the number of coefficients, 45, and the reference of the apnoea episode starting at around the 150th sample, the system only takes about 33 samples to fully detect the lack of chest movement.

Thus, the total delay to detect a lack of chest movement is $\frac{33}{10Hz} + \frac{45}{10Hz} = 7.8 \text{ seconds}$ in this concrete case. This delay results in a very good and fast adaptation to the apnoea episodes, taking into account that those episodes are given in periods of lack of respiration of 20 seconds or more.

In the same way, we return to the breathing state quite fast, but this time falling in a higher respiratory rate at 0.5Hz, which could be considered a fact of interest.

Further analysis on those type of patterns, were the respiratory rate is above the normal, is purposed in the following case of study. This is a measured case where we force a shortness of breath period, normally associated to tachycardia episodes:

Technique	LMS
Target Frequency	0.3 Hz (from 0 - 200) 1 Hz (from 200 - 350) 0.5 Hz (from 350 - 500)
p	45
μ	2
Initialization	Vector of zeros

Table 20: LMS algorithm setup for respiratory patterns (shortness of breath associated to tachycardia) detection parameters, laboratory

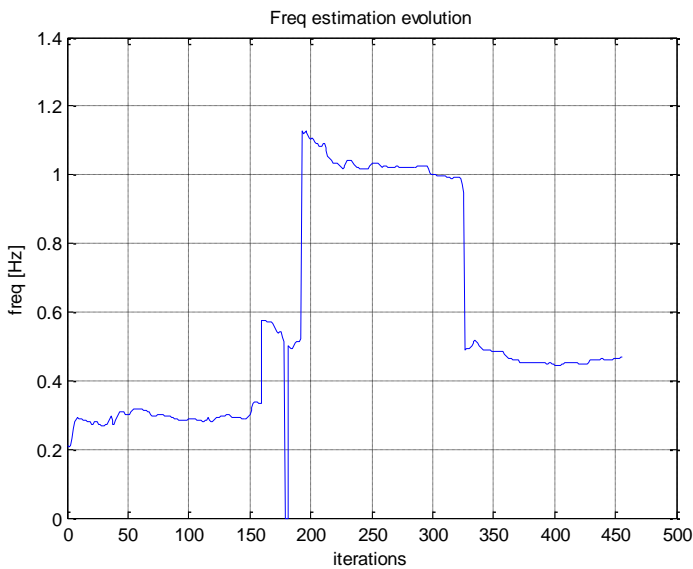


Fig 46: Frequency estimation evolution of LMS algorithm, laboratory

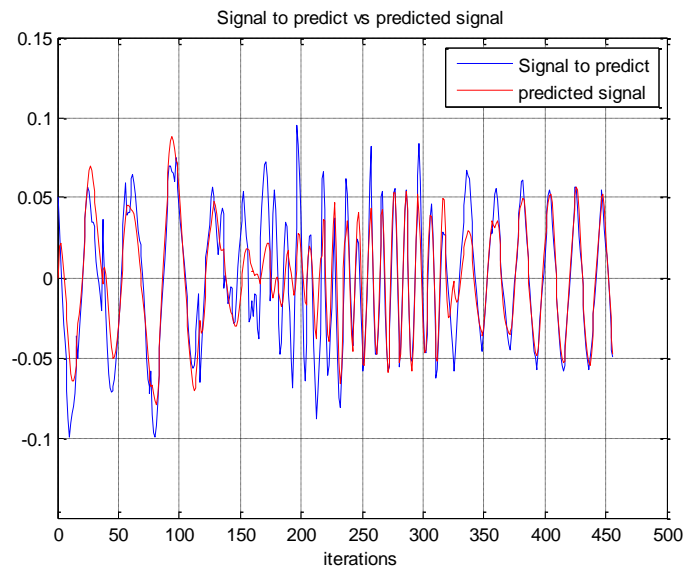


Fig 47: Signal to predict in comparison with predicted signal, laboratory

In the above Figures 46 and 47 we present the results for a different respiratory pattern following the configuration in table 20. In this case, and with the same estimator parameters as in the past situation, we are able to detect the shortness of breath (high respiratory rate) often associated with a tachycardia episode.

In this case the response of the system is quite fast even though we have some instabilities at the beginning of the episode probably due the movement in the patient, as we can see in the predicted signal in Figure 47. This results show off the flexibility of the system in front of different situations and applications

Seeing table 19 and 20, the configuration of the algorithm, we can highlight the update step set up at its theoretical boundary, and also, the number of coefficients is increased. Both this modifications shape up the algorithm to a quick response even though we might lose some precision. Given the main target of this system being the rapid detection of respiratory pattern episodes, it seems a fair trade-off losing a little precision in the steady measurement in exchange of a quicker response.

5. Budget

Time computation	HW and API interaction	Software simulation	Signal processing to obtain breath rate	Apnoea/Respiratory patterns detection	Total
Time (Hours)	21	20	28	33	102
Breakdown	3h*7 weeks	4h*5 weeks	4h*7 weeks	3h*11 weeks	

Considering 35 €/hour, for an amount of 102 hours, the price for the labour of a Jr Engineer to complete this project is approximately **3570 €**.

Prototyping cost	type	items	Cost
	Licences		
		Matlab	500 €
	HW		
		1 unity of the Pulson 410 Series	2500 €
	Labour		
		102 hrs of Jr Engineer	3570 €
		Total	6570 €

The final cost of the prototyping of the product would be around **6570 €**. The elevated price for the HW device is related its exclusiveness, given that nowadays there are not so many companies selling UWB devices of this characteristics for research purposes.

6. Conclusions and future development:

In this thesis we have presented a complete system able to detect respiratory rate of a patient in a complete non-invasive and non-movement restrictive way. Moreover and specially, this system is also able to detect respiratory patterns as apnoea episodes and short breathing usually associated with tachycardia episodes. We have been able to fulfil the objectives, highlighting the agility of the system to track and detect different respiratory patterns with accuracy.

We start the process of designing the detector system by defining its structure. Following that, we focus on obtaining a reliable and coherent set of simulations to test and develop our first algorithms. Then, once we have the different estimators working in the simulated scenario, we have set up two different experimental environments to further test and adjust our approaches. Finally, in the real experiment scenario we focus our efforts in obtaining frequency variant measurements to calibrate our adaptive algorithms to the most suitable response to our problem.

There have been issues and setbacks to resolve, which have delayed some parts of the development. Particularly the configuration of the hardware device has been challenging at some points, but in the end we have gained deep insights of it, allowing us to understand and obtain the desired data from it.

As future development of this thesis there are plenty of complementary applications that would lead us to a more complete and reliable overall system. For example, an algorithm to track the position of a moving patient in a room would enable home monitoring in dynamic situations (maybe with a multistatic radar application, also implementable with the Pulson 410 devices). Another highly interesting approach would be to additionally track heartbeat of the patients as presented in some studies, like in [9], and combine it with our algorithm to detect heart arrhythmias.

As a final reflexion of this thesis, I value in a high measure all the different processes and phases in which I have been involved during this project. From the design, first implementations (with different signal processing techniques and methods) and simulations (with channel modelling research and implementation), to deal directly with the hardware until obtain the final fully functional system. In the end, the obtained final wireless system is composed by a set of well-known tools, but this combination of simple tools leads to the resolution of a new problematic in terms of application and technology.

Bibliography:

- [1] R. Z. Morawski, Y. Yashchyshyn, R. Brzyski, F. Jacobsen, W. Winiecki. "On applicability of impulse-radar sensors for monitoring of human movements". *20th IMEKO TC4 International Symposium and 18th International Workshop on ADC Modelling and Testing Research on Electric and Electronic Measurement for the Economic Upturn*, 15-17 September, 2014, Benevento, Italy. pp. 754-759. ISBN-14: 978-92-990073-2-7.
- [2] National Institutes of Health, Consensus Development Conference on Infantile Apnea and Home Monitoring, Sept 29 to Oct 1, 1986. *Pediatrics*. 1987;79:292–299
- [3] Christopher Voscopoulos, Diane Ladd, Lisa Campana, Edward George. "Non-Invasive Respiratory Volume Monitoring to Detect Apnea in Post-Operative Patients: Case Series" *J Clin Med Res*. 2014;6(3):209-214. doi: <http://dx.doi.org/10.14740/jocmr1718w>
- [4] Institute of Medicine (US) Committee on Understanding Premature Birth and Assuring Healthy Outcomes; Behrman RE, Butler AS, editors. *Preterm Birth: Causes, Consequences, and Prevention*. Washington (DC): National Academies Press (US); 2007. Available from: <http://www.ncbi.nlm.nih.gov/books/NBK11362/>
- [5] Grenvik, A., Ballou, S., McGinley, E., Millen, J., Cooley, W.L., Safar P. (1972) *Impedance Pneumography: Comparison between Chest Impedance Changes and Respiratory Volumes in II Healthy Volunteers*. *Chest*. October 1972;62(4):439-443
- [6] R. Farré, J. M. Montserrat, D. Navajas *Eur Respir J*. *Noninvasive monitoring of respiratory mechanics during sleep*. 2004 December; 24(6): 1052–1060. doi: 10.1183/09031936.04.00072304
- [7] Othman, M.A.; Sinnappa, M.; Azman, H.; Aziz, M.Z.A.A.; Ismail, M.M.; Hussein, M.N.; Sulaiman, H.A.; Misran, M.H.; Said, M.A.M.; Ramlee, R.A.; Jack, S.P.; Ahmad, B.H. "5.8 GHz microwave Doppler radar for heartbeat detection", *Radioelektronika (RADIOELEKTRONIKA)*, 2013 23rd International Conference, On page(s): 367 – 370
- [8] Lubecke, O. B., P. W. Ong, and V. M. Lubecke, "10 GHz Doppler radar sensing of respiration and heart movement," *2002 IEEE Proceedings of the IEEE 28th Annual Northeast Bioengineering Conference*, 55-56, Apr. 20-21, 2002.
- [9] A. Lazaro, D. Girbau, and R. Villarino, "Analysis of vital signs monitoring using an ir-UWB radar," *Progress In Electromagnetics Research*, Vol. 100, 265-284, 2010. doi:10.2528/PIER09120302
- [10] E. M. Staderini, "UWB radars in medicine", *IEEE Aerospace and Electronic Systems Magazine*, Vol. 17, No. 1, pp. 13 - 18, Jan. 2002.
- [11] Venkatesh, S., C. Anderson, N. V. Rivera, and R. M. Buehrer, "Implementation and analysis of respiration-rate estimation using impulse-based UWB," *2005 IEEE Military Communications Conference (IEEE Milcom'05)*, Vol. 5, 3314-3320, Oct. 2005.
- [12] H. C. So, K. W. Chan, Y. T. Chan, and K. C. Ho, "Linear prediction approach for efficient frequency estimation of multiple real sinusoids: algorithms and analyses," *IEEE Trans. Signal Process.*, vol. 53, no. 7, pp. 2290–2305, July 2005.
- [13] Bartlett, M.S. (1948). "Smoothing Periodograms from Time-Series with Continuous Spectra". *Nature* 161: 686–687. doi:10.1038/161686a0
- [14] F.S. Schlindwein, D.H. Evans, "Autoregressive spectral analysis as an alternative to fast Fourier transform analysis of Doppler ultrasound signals", in: E. Arnold (Ed.), *Diagnostic Vascular Ultrasound* 8, 1992, pp. 74–84.
- [15] S. S. Haykin, *Adaptive Filter Theory*, 2nd ed. Englewood Cliffs, NJ: Prentice-Hall, 1991
- [16] B. Widrow, J. R. Glover, Jr., J. M. McCool, J. Kaunitz, C. S. Williams, R. H. Hearn, J. R. Zeidler, E. Dong, Jr., and R. C. Goodlin. "Adaptive noise cancelling: Principles and applications." *Proc. IEEE*, vol. 63, no. 12, pp. 1699–1716, Dec. 1975: A
- [17] Yule, G. Udny (1927) "On a Method of Investigating Periodicities in Disturbed Series, with Special Reference to Wolfer's Sunspot Numbers", *Philosophical Transactions of the Royal Society of London*, Ser. A, Vol. 226, 267–298.
- [18] Jump up^ Walker, Gilbert (1931) "On Periodicity in Series of Related Terms", *Proceedings of the Royal Society of London*, Ser. A, Vol. 131, 518–532.
- [19] Vega, Leonardo Rey, Rey, Hernan, *A Rapid Introduction to Adaptive Filtering (SpringerBriefs in Electrical and Computer Engineering)*. Springer Publishing Company, Incorporated ©2012
- [20] J. Lai, Y. Xu, E. Gunawan, E. Chua, A. Maskooki, Y. L. Guan, K.-S. Low, C. B. Soh, and C.-L. Poh, "Wireless sensing of human respiratory parameters by low power ultrawideband impulse radio radar," *IEEE Trans. Instrum. Meas.*, vol. 60, no. 3, pp. 928–938, Mar. 2011.

- [21] S. Gezici, "Theoretical limits for estimation of periodic movements in pulse-based UWB systems," *IEEE J. Select. Topics Signal Process.*, vol. 1, no. 3, pp. 405–417, Oct. 2007.
- [22] S. Gezici and O. Ankan, "Theoretical limits and a practical estimator for joint estimation of respiration and heartbeat rates using UWB impulse radio," in *Proc. IEEE Int. Conf. Ultra-Wideband*, Sep. 2007, pp. 606–611
- [23] A. F. Molisch et al., IEEE 802.15.4a channel Model—Final report Tech. Rep. Doc. IEEE 802.15-04-0662-02-004a, 2005.
- [24] <http://es.mathworks.com/help/signal/ref/gauspuls.html>

Appendices (optional):

DFT calculation of the clutter removed signal:

Given that $x[n, m]$ has two temporal axis, we have to apply the spectral analysis in the dimension in which our variation of interest progresses (chest movement). As can be seen from equation (4), the chest movement only depends on the slow time (n), so we apply our analysis along that dimension:

$$X[k, m] = \sum_{n=0}^{Ns-1} x[n, m] e^{-\frac{j2\pi kn}{Ns}} = \alpha_b \sum_{n=0}^{Ns-1} \frac{p[m - m_b[n]]}{a(n, m)} e^{-\frac{j2\pi kn}{Ns}} - x_0(m) \delta_D(k) \quad (37)$$

With $\delta_D(k)$ being the Dirac delta function and $x_0(m)$ the residual term from equation (8), which does not depend on the slow time. The auxiliary term $a(n, m)$ can be rewritten in terms of its DFT over the fast-time m :

$$\begin{aligned} A[n, l] &= \sum_{m=0}^{Nf-1} a[n, m] e^{-\frac{j2\pi lm}{Nf}} = \sum_{m=0}^{Nf-1} p[m - m_b[n]] e^{-\frac{j2\pi lm}{Nf}} \\ &= e^{-j2\pi l m_b[n]} \sum_{m=0}^{Nf-1} p[m] e^{-\frac{j2\pi lm}{Nf}} = e^{-j2\pi l m_b[n]} P(l) \end{aligned} \quad (38)$$

Where $P(l)$ is the DFT of the transmitted pulse $p(m)$ over the fast time frequency axis. Therefore, if we go backwards and we do the inverse Fourier transform of $A[n, l]$ we obtain a new expression for $a[n, m]$:

$$a[n, m] = \frac{1}{Nf} \sum_{l=0}^{Nf-1} P(l) e^{\frac{j2\pi l(m - m_b[n])}{Nf}} \quad (39)$$

Replacing (12) in (10) we obtain:

$$\begin{aligned} X[k, m] &= \alpha_b \sum_{n=0}^{Ns-1} \left[\frac{1}{Nf} \sum_{l=0}^{Nf-1} P(l) e^{\frac{j2\pi l(m - m_b[n])}{Nf}} \right] e^{-\frac{j2\pi kn}{Ns}} - x_0(m) \delta_D(k) \\ &= \frac{\alpha_b}{Nf} \sum_{l=0}^{Nf-1} P(l) \underbrace{\sum_{n=0}^{Ns-1} e^{-\frac{j2\pi l m_b[n]}{Nf}} e^{-\frac{j2\pi kn}{Ns}} e^{\frac{j2\pi lm}{Nf}}}_{Z[k, l]} - x_0(m) \delta_D(k) \end{aligned} \quad (40)$$

In our case, with the respiratory rate signal being sinusoidal as defined in equation (4), we can develop the factor $Z[k, l]$:

$$\begin{aligned}
 Z[k, l] &= \sum_{n=0}^{Ns-1} e^{\frac{-j2\pi l m_b[n]}{N_f}} e^{\frac{-j2\pi k n}{N_s}} \\
 &= \sum_{n=0}^{Ns-1} e^{\frac{-j2\pi l(m_0 + m_d \sin(2\pi f_b n))}{N_f}} e^{\frac{-j2\pi k n}{N_s}} \\
 &= e^{\frac{-j2\pi l m_0}{N_f}} \sum_{n=0}^{Ns-1} e^{\frac{-j2\pi l m_d \sin(2\pi f_b n)}{N_f}} e^{\frac{-j2\pi k n}{N_s}}
 \end{aligned} \tag{41}$$

At this point we have to deal with the factor $e^{\frac{-j2\pi l m_d \sin(2\pi f_b n)}{N_f}}$. To do so, a function with the shape of $e^{j\gamma \sin(2\pi f_b n)}$ can be expanded as a series of Bessel Functions in the following way:

$$e^{-j\gamma \sin(2\pi f_b n)} = \sum_{q=-\infty}^{\infty} J_q(\gamma) e^{-j2\pi q f_b n} \tag{42}$$

Therefore, applying (15) to (14) yields:

$$\begin{aligned}
 Z[k, l] &= e^{\frac{-j2\pi l m_0}{N_f}} \sum_{q=-\infty}^{\infty} J_q(\gamma) \sum_{n=0}^{Ns-1} e^{-j2\pi q f_b n} e^{\frac{-j2\pi k n}{N_s}} \\
 &= e^{\frac{-j2\pi l m_0}{N_f}} \sum_{q=-\infty}^{\infty} J_q(\gamma) \sum_{n=0}^{Ns-1} e^{-j2\pi(\frac{k}{N_s} + q f_b)n} = e^{\frac{-j2\pi l m_0}{N_f}} \sum_{q=-\infty}^{\infty} J_q(\gamma) \delta_D\left(\frac{k}{N_s} + q f_b\right)
 \end{aligned} \tag{43}$$

Where $\gamma = \frac{2\pi l m_d}{N_f} = \frac{\beta l}{N_f}$ and where subsequently $\beta = 2\pi m_d$. Replacing (16) into (13) we obtain:

$$X[k, m] = \alpha_b \sum_{q=-\infty}^{\infty} \delta_D\left(\frac{k}{N_s} + q f_b\right) \Omega_q(m) - x_0(m) \delta_D(k) \tag{44}$$

With the auxiliary expression being

$$\Omega_q(m) = \frac{1}{N_f} \sum_{l=0}^{N_f-1} J_q\left(\frac{\beta l}{N_f}\right) P(l) e^{\frac{j2\pi l(m-m_0)}{N_f}} \tag{45}$$

It can be verified that $|\Omega_l(m)|$ is maximized for $m = m_0$:

$$\Omega_q(m_0) \triangleq G_q(\beta) = \frac{1}{N_f} \sum_{l=0}^{N_f-1} J_q\left(\frac{\beta l}{N_f}\right) P(l) \tag{46}$$

Finally, manipulating the result from equation (44) we obtain:

$$\begin{aligned}
 X[k, m] &= \alpha_b \sum_{q=-\infty}^{\infty} \delta_D\left(\frac{k}{N_s} + qf_b\right) \Omega_q(m) - x_0(m) \delta_D(k) \\
 &= \alpha_b \sum_{q=-\infty, q \neq 0}^{\infty} \delta_D\left(\frac{k}{N_s} + qf_b\right) \Omega_q(m) + (\alpha_b \Omega_0(m) - x_0(m)) \delta_D(k)
 \end{aligned} \tag{47}$$

And for the optimal value of m :

$$X[k, m_0] = \alpha_b \sum_{q=-\infty, q \neq 0}^{\infty} \delta_D\left(\frac{k}{N_s} + qf_b\right) G_q(\beta) + (\alpha_b G_0(\beta) - x_0(m_0)) \delta_D(k) \tag{48}$$

From the expression (47), we see that the DFT along slow-time comprises a train of impulses at the harmonics of the respiration frequency f_b . The magnitude of the harmonics in $|X[k, m]|$ are determined by m , β and $P(l)$ and the maximum value is obtained at $m = m_0$ as seen in equation (46).

Due to the spectral leakage of the DFT, we apply a window, therefore, we convolve the result of the equation (48) with the intrinsic DFT rectangular window of structure:

$$\varphi(n) = \text{rect}\left(\frac{n}{N_s}\right) \tag{49}$$

Which in frequency domain translates to:

$$\phi(f) = N_s \text{sinc}(nN_s) \tag{50}$$

Applying the convolution to equation (48):

$$\begin{aligned}
 X_w[k, m_0] &= X[k, m_0] * \phi(k) \\
 &= \alpha_b \sum_{q=-\infty, q \neq 0}^{\infty} \phi\left(\frac{k}{N_s} + qf_b\right) G_q(\beta) + (\alpha_b G_0(\beta) - x_0(m)) \phi(k)
 \end{aligned} \tag{51}$$

As previously mentioned, all this study was neglecting the noise. If we now assume additive white Gaussian noise like:

$$n(n, m) \sim N(0, \sigma_n^2 \delta_D(n) \delta_D(m)) \tag{52}$$

The output of the motion filter from (51) looks like:

$$\begin{aligned}
 X'_w[k, m_0] &= \alpha_b \sum_{q=-\infty, q \neq 0}^{\infty} \phi\left(\frac{k}{N_s} + qf_b\right) G_q(\beta) + \\
 &(\alpha_b G_0(\beta) - x_0(m)) \phi(k) + N(k, m_0) * \phi(k)
 \end{aligned} \tag{53}$$

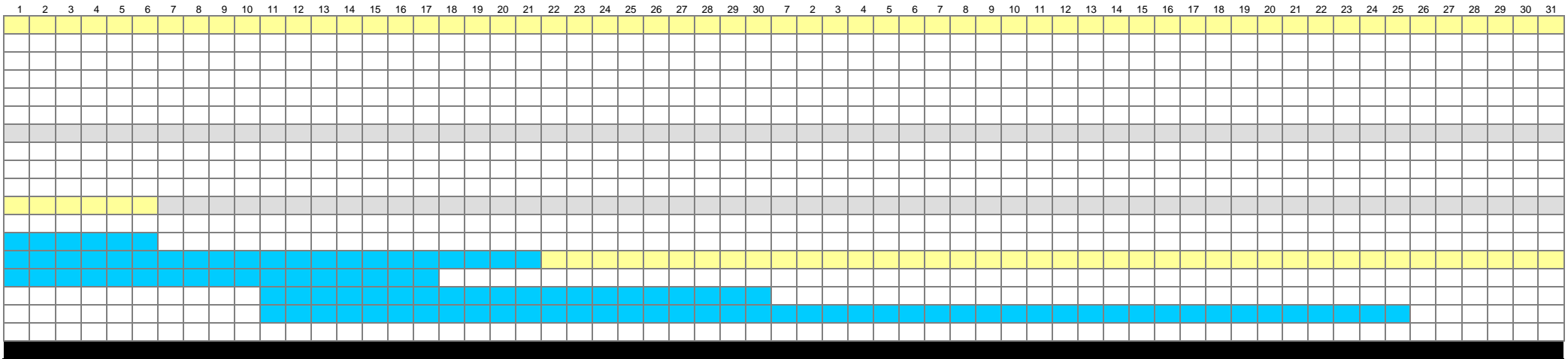
With the new factor:

$$N(k, m) = \sum_{n=0}^{N_s-1} n(n, m) e^{-\frac{j2\pi kn}{N_s}} \quad (54)$$



Jun

Jul



Sept

